Sep 10

Electromagnetic Field Study

The prediction of electromagnetic fields generated by submarine power cables.

Prepared by
Michael Slater, Science Applications International Corp.
Richard Jones, ENS Consulting
Dr. Adam Schultz, consultant
on behalf of Oregon Wave Energy Trust

This work was funded by the Oregon Wave Energy Trust (OWET). OWET was funded in part with Oregon State Lottery Funds administered by the Oregon Business Development Department. It is one of six Oregon Innovation Council initiatives supporting job creation and long-term economic growth.

Oregon Wave Energy Trust (OWET) is a nonprofit public-private partnership funded by the Oregon Innovation Council. Its mission is to support the responsible development of wave energy in Oregon. OWET emphasizes an inclusive, collaborative model to ensure that Oregon maintains its competitive advantage and maximizes the economic development and environmental potential of this emerging industry. Our work includes stakeholder outreach and education, policy development, environmental assessment, applied research and market development.

Record of Revisions

Revision	Date	Section and Paragraph	Description of Revision
Original	September 2010	All	Initial Release

TABLE OF CONTENTS

TABLE OF FIGURES

TABLE OF TABLES

1. EXECUTIVE SUMMARY

This report describes the emissive characteristics of electromagnetic (EM) fields from submerged power cables in the marine environment. This study was commissioned with the goal of analyzing and synthesizing the expected EM field levels near energized power cables and wave energy conversion devices in the coastal environment.

The basic physical theory was derived from fundamental laws of electrical current and magnetism. Then, the boundary conditions were applied to determine the local EM field effects from energized cables that were representative of the subsea cable industry. First, a model was derived to predict the electromagnetic fields produced by DC monopole and bipole power cables. Next, a transmission line model was developed to quickly and accurately determine the electromagnetic fields surrounding an AC cable as a function of distance from the cable using the cable construction, the power frequency, and phase current. The AC model was developed for both single phase and trefoil three phase cables, with either individual phase shields, or with a single shield that encompasses all three phases. The model was verified using Finite Element Analysis. The model successfully predicted the fields measured and recorded in a baseline assessment of EMF for an offshore wind farm [1]. Therefore, a transmission line model will reasonably predict the fields generated around specific cable designs being considered for subsea power transmission.

Finally, this work has shown that accurate measurements of the fields adjacent to power cables requires knowledge of the location of the sensors relative to the cable as the fields decrease rapidly with distance from the cables.

2. INTRODUCTION

2.1 Purpose

This report estimates the localized electromagnetic field (EMF) strength values created by energized submarine power cables. The purpose of this report is to define analytic methods for predicting the electric and magnetic fields produced by DC cables (single and bipole) and AC cables (single and three phase), and then to predict the effect of cable burial on these fields. The focus of this report is to identify the expected range of values of electromagnetic signals created by submerged power cables in the near shore marine environment, and compare the expected results to those found in other literature on the subject.

2.2 Background

The Oregon Wave Energy Trust (OWET) was formed in 2007 to coordinate the development of power generation from offshore wave energy with the objective of generating 500 MW along the Oregon coast by 2025. The generated power will be transmitted to shore using subsea power cables to enable local or national distribution. The transmission of high power along such cables will induce both electric and magnetic fields into the sea, which may disturb marine species such as sharks and rays, which are sensitive to electromagnetic fields. Together with estimated or measured ambient EMF noise conditions, predictive results from this report can be used to estimate the environmental effects of placing such EM fields in the near shore environment.

2.3 Report Organization

This report has ten topical sections and five supporting appendices. The first three sections contain the executive summary, the introduction, which describes the project motivation and background, and a survey of prior work on this subject. Section 4 describes the methodology of analysis. The fundamental physical theories outlined in Section 5 serve as the basis for understanding the subsequent modeling analysis. Sections 6 (DC) and 7 (AC) present the development of models for various cable types. The use of these models applied to the special condition of buried cable is given in Section 8. Section 9 compares the modeled results to actual measurements made of a submarine cable crossing in the UK. Overall conclusions are presented in Section 10. Appendix A contains a glossary of mathematical symbols used in this report,

Appendix B provides an acronym list. Appendix C describes the physical phenomenon of skin depth. Physical details of the cables described in Section 9 are shown in Appendix D. Appendix E contains the bibliography of references.

3. PRIOR ART

Collaborative Offshore Wind Research into the Environment (COWRIE), Ltd is a registered charity in the UK governed by a Board of Directors drawn from The Crown Estate, the Department for Energy and Climate Change (DECC), and the British Wind Energy Association (BWEA). The purpose of the organization is to advance and improve the understanding and knowledge of potential environmental impacts of offshore wind farm development in UK waters.

COWRIE commissioned a study of the electromagnetic fields generated by submarine power cables, which was undertaken by the Centre for Marine and Coastal Studies (CMACS, 2003). This work used Finite Element Analysis (FEA) to predict the electromagnetic fields around a cable, which required little understanding of the underlying physical process, and generation of a new model for each cable, or environment, to be analyzed. Although attractive field plots can be produced with commercially available FEA software, this approach can be cumbersome and perhaps unnecessary, as analytic solutions are possible. Further, the electric field in the seawater, or seabed, was not determined directly from the FEA analysis, but derived from the predicted magnetic field. However, the equations presented by CMACS for calculating the electric field in this way appear to be incorrect. The COWRIE report states that the electric and magnetic fields are related by the following expression:

$$E = 2\pi f B$$

Where:

E = electric field (V/m)

f = power frequency (Hz)

B = magnetic field (tesla)

The dimensions, or units, of this equation do not balance, unless the E field has units of V/m^2 rather than V/m, resulting in what appears to be an anomaly in the mathematical development. Otherwise, the report is a good starting point on the subject and is the original work from which the current undertaking was initiated.

4. METHODOLOGY

Two primary cable types were modeled using basic electromagnetic theories: direct current (DC) and alternating current (AC) cables. First, a single conductor cable was analyzed, from which other conditions were derived. Next, two distinct DC cable models were considered. The first was a single DC cable with a seawater return path of the type commonly used in the telecommunications industry. The second was a two-conductor or bi-pole cable, with positive voltage on one conductor, and a return path on the other. Three types of AC cable were modeled. The first was a simple two-conductor cable using a single phase of alternating current. Two variants of a three conductor (trefoil) cable were analyzed, one with individually shielded conductors, and the other with an overall shield surrounding the trefoil cable bundle.

While these models may not cover every possible combination of cable type encountered, they do demonstrate the capability to create analytical models that predict the range of magnitude of EMF values of an energized cable. Further, they provide a basic toolset from which additional variations could be created, subject to the imagination of cable designers. For each development, assumptions are stated, and mathematical expressions provided as the primary technical descriptor of the analyses.

Readers are reminded that the modeled predictions for this work assume a simplified model, including the relatively homogeneity of the water and substrate conditions. Research into EMF generation and propagation has demonstrated that a variety of factors, such as topographic, bathymetric, and geologic conditions, contribute to the natural generation and propagation of EM fields, particularly for the near-shore environment. However, these conditions are not mathematically described herein. Thus, caution is urged when applying these predictive results to a specific environment.

5. BASIC THEORY

Two fundamental relationships describe the magnetic and electric fields generated by an electrical conductor in a given medium. To simplify the analysis, it is assumed that the relative permeability (μ_r) and relative permittivity (ε_r) of the media are constant. The magnetic field (B) as a function of distance (r) from the center of a conductor carrying a current I, can be derived from Ampere's Law:[1]

$$B(r) = \frac{I\mu_0\mu_r}{2\pi r} \quad 1)$$

Where I = current in amps

μ_0 = permeability of free space ($4\pi \times 10^{-7}$ N/A^2)

μ_r = relative permeability of medium (~1 for non ferromagnetic materials)

Similarly, the electric field surrounding a line charge can be derived from Gauss's Law:[2,3]

$$E(r) = \frac{q}{2\pi r\varepsilon_0\varepsilon_r} \quad 2)$$

Where q = charge/unit length (coulomb/m)

ε_0 = permittivity of free space (8.66×10^{-12} F/m)

ε_r = relative permittivity of material surrounding line charge (1 for air)

[1] http://farside.ph.utexas.edu/teaching/316/lectures/node75.html

[2] http://en.wikipedia.org/wiki/Gauss's_law

[3] http://35.9.69.219/home/modules/pdf_modules/m133.pdf

6. DIRECT CURRENT CABLES

This section describes simple analytic models for determining the magnitude of the electric and magnetic fields produced by single and bipole DC submarine cables.

6.1 Single Conductor DC Cable

Consider an unshielded DC conductor insulated with polyethylene, carrying a current *I* amps at a voltage V_C volts, with the cable immersed in seawater (see Figure 1).

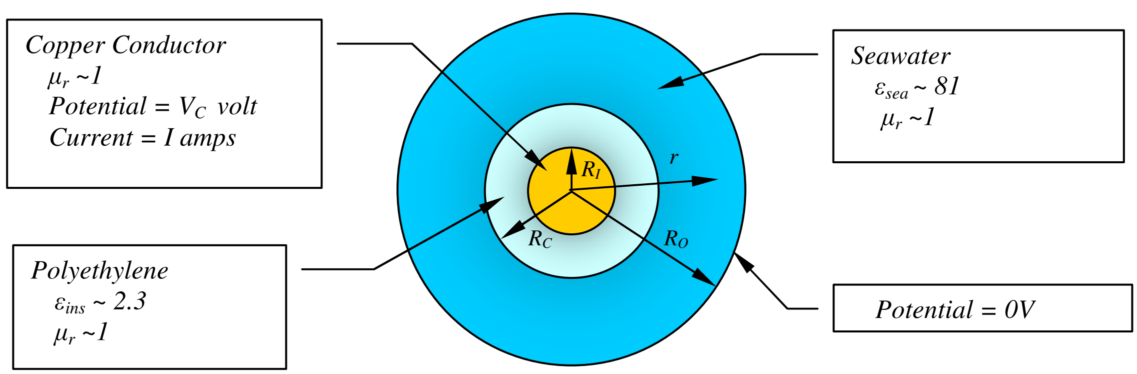

Figure 1 – Model for a Single DC Conductor in the Sea

The highest electric fields can be expected to reside within the dielectric with the lowest permittivity, which in all practical cases will be the cable insulation. To determine the electric field within the sea, the potential at the interface between the cable insulation and seawater must first be determined using the classical capacitor divider equation.

$$V_{SEA} = \frac{V_C C_{INS}}{C_{INS} + C_{SEA}} \qquad 3)$$

Where C_{INS} = Capacitance of the cable insulation (F/m)

C_{SEA} = Capacitance of the sea (F/m)

These capacitances are determined using the well-known equations for coaxial conductors.

$$C_{INS} = \frac{2\pi\varepsilon_0\varepsilon_{INS}}{\ln\left(\frac{R_C}{R_I}\right)} \qquad \text{and} \qquad C_{SEA} = \frac{2\pi\varepsilon_0\varepsilon_{SEA}}{\ln\left(\frac{R_O}{R_C}\right)}$$

Where ε_0 = permittivity of free space ($4\pi \times 10^{-7}$ N/A^2)

R_C, R_I, R_O, ε_{INS}, and ε_{SEA} are as defined in **Figure 1** [4,5]

The electric fields within the sea and cable insulation are coaxial fields, which are given by equations 4) and 5) respectively:

$$E_{SEA}(r) = \frac{V_{SEA}}{r\ln\left(\frac{R_O}{R_C}\right)} \qquad \text{where } r > R_C \qquad 4)$$

$$E_{INS}(r) = \frac{V_C}{r\ln\left(\frac{R_C}{R_O}\right)} \qquad \text{where } R_I < r < R_C \qquad 5)$$

The maximum magnetic field around the cable is given by:

$$B(r) = \frac{I\mu_0\mu_r}{2\pi r} + B_{earth} \qquad 6)$$

Where μ_r = permeability of medium (= 1 for seawater and polymers)

B_{earth} = 50 μT (typically between 30 and 60 μT) [6]

The resulting electric and magnetic fields for an arbitrary cable design detailed in Table 1, have been calculated for a normalized line current of 1 A and potential of 1 V, and the results are shown in Figure 2 and Figure 3.

[4] http://www.kayelaby.npl.co.uk/general_physics/2_6/2_6_5.html

[5] http://www.kayelaby.npl.co.uk/general_physics/2_6/2_6_6.html

[6] http://en.wikipedia.org/wiki/Earth's_magnetic_field#Field_characteristics

Table 1 – Properties of an Arbitrary Unshielded DC Cable

Parameter	Value
Conductor diameter (mm)	50
Insulation Diameter (mm)	100
Permittivity of insulation	2.3
Permittivity of sea	81
Max DC Current (A)	1000
Conductor resistance (ohm)	1

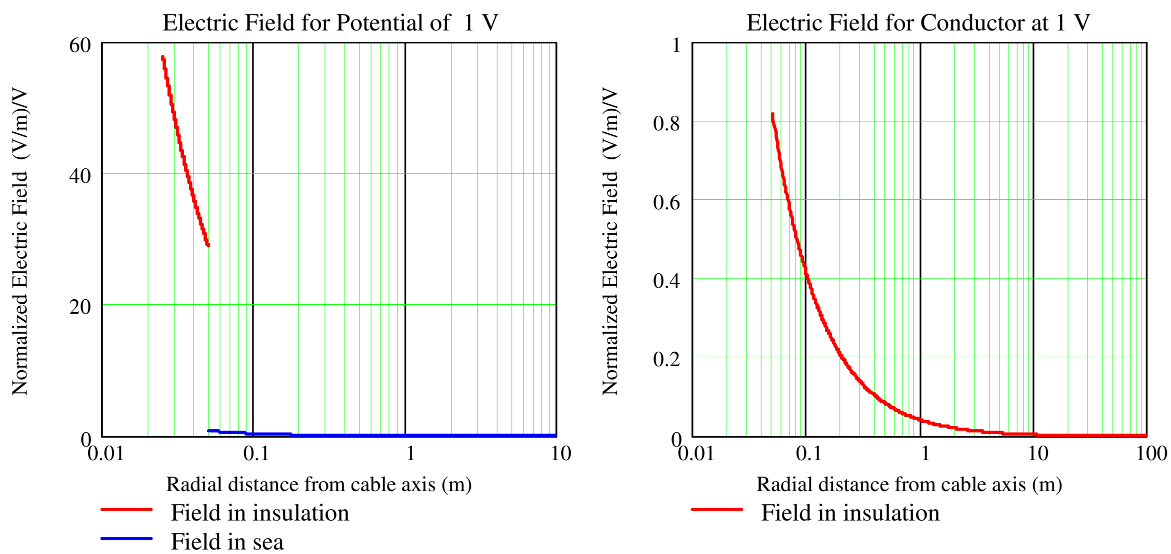

Figure 2 – Normalized Electric Field Generated by Potential of 1V on Conductor

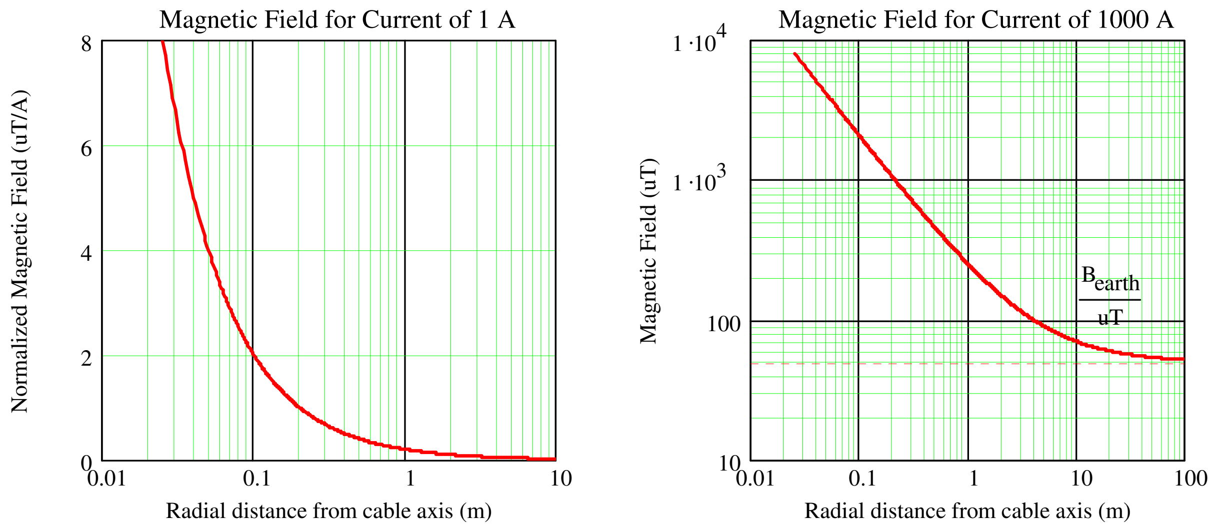

Figure 3 – Normalized B Field and Absolute B Field for a Current of 1000 A

If a perfectly grounded metallic shield is applied over the insulation, then the electric field will be contained solely within the insulation. However, the magnetic field in the sea will not be attenuated by the shield, as the magnetic field is time invariant (i.e. DC conditions).

If this magnetic field is induced in *flowing* seawater, then an electric field will be induced in the sea by magneto-hydrodynamic (MHD) generation (Figure 4), and the maximum electric field is given by:

$$E_{MHD}(r) = B(r)v$$

Where v = water flow velocity (m/s)

$B(r)$ = peak magnetic field at a distance r from cable (T)

Substitution into equation 1) gives:

$$E_{MHD}(r) = B(r)v = \frac{I\mu_0\mu_r v}{2\pi r} \qquad 7)$$

This MHD induced electric field is additive to the electric field generated by seawater moving though the earth's magnetic field, therefore the maximum electric field is given by:

$$E_{\max}(r) = \left(B(r) + B_{earth}\right).v = \left(\frac{I\mu_0\mu_r}{2\pi r} + B_{earth}\right).v \qquad 8)$$

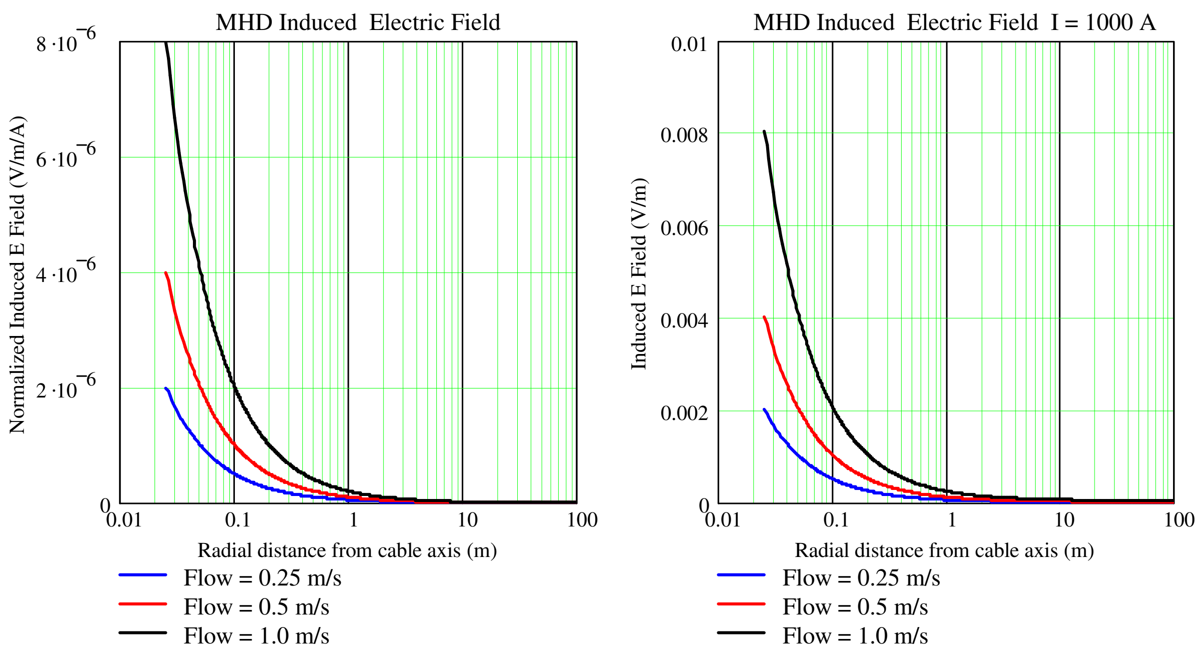

Figure 4 – MHD Electric Fields Generated in Sea by Seawater Flow Across Cable

6.2 Single DC Conductor, Sea-Earth Return

If a single DC power cable is adopted, then the circuit must be completed via the sea using an anode and cathode. High electric fields can occur in the sea close to an electrode from current convergence at the electrode and the electrode resistance. Consider the power transmission system as seen in Figure 5.

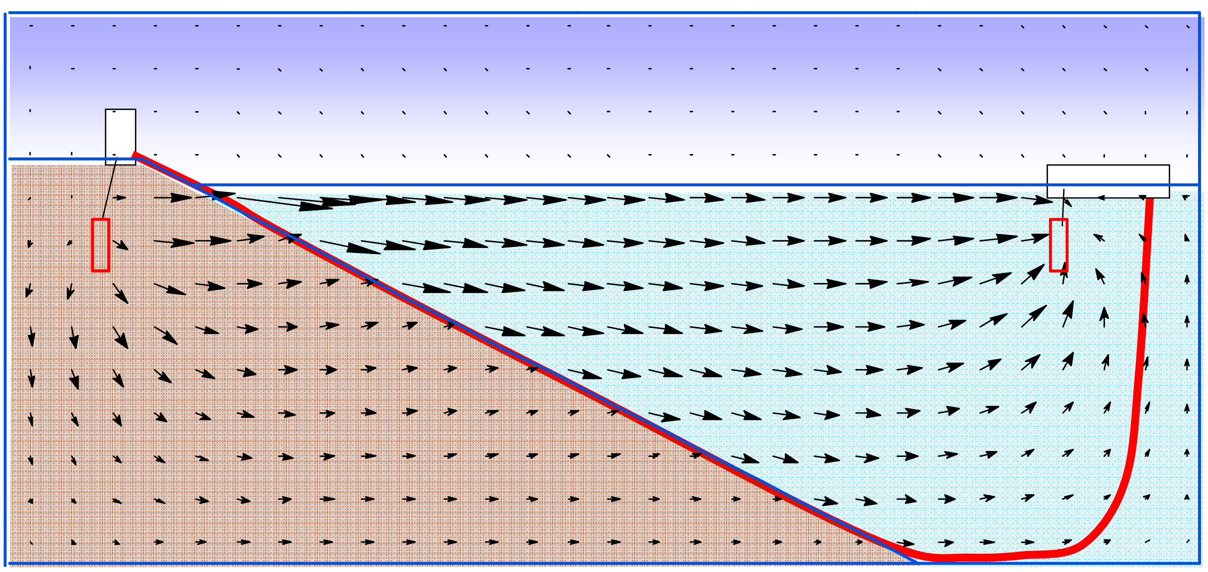

Figure 5 – Schematic of Single Cable DC Power Transmission

The anode of the system is usually located on land and consists of multiple electrodes embedded in coke breeze to give a low electrode resistance. If the cathode is a cylinder, then the resistance of the electrode to the sea (also referred to as the electrode resistance) can be calculated as follows:

If only one end of the cylindrical cathode is exposed to the sea, then the electrode resistance (R_{cath}) is given by the following surface integral:

$$R_{cath} = \int_{r_o}^{r_1} \frac{\rho}{2\pi r l + \pi r^2} dr = \frac{\rho}{2\pi l}\left[\ln(r) - \ln(l+r)\right]_{r_0}^{r_1}$$

$$= \frac{\rho}{2\pi l}\ln\left(\frac{r_1(2l+r_0)}{r_0(2l+r_1)}\right) \qquad 9)$$

where: l = length of electrode (m)

r_0 = radius of electrode (m)

ρ = resistivity of seawater (~ 0.25 Ω.m)

r_1 = distance from electrode axis (m)

If $r_1 >> l$ equation 5) reduces to:

$$R_{cath} = \frac{\rho}{2\pi l}\left[\ln\left(\frac{2l+r_0}{r_0}\right)\right] = \frac{\rho}{2\pi l}\left[\ln\left(\frac{4l}{d}+1\right)\right] \qquad 10)$$

Where d = diameter of electrode (m)

It should be noted that if the distance between the two remote electrodes is greater than 100 times the radius or length of the electrodes (actual case for a sea ground return), then the resistance of the electrolyte (*i.e.* the sea resistance) is very small and may be neglected.

The electrode resistance as a function of length is shown in Figure 6 for various electrode diameters and a typical seawater resistivity of 0.25 ohm·m. From this graph it is seen that if the cathode diameter is 6 inches, then it must be ≥ 1.5 m long to give a resistance to the sea of ≤ 0.1 ohms

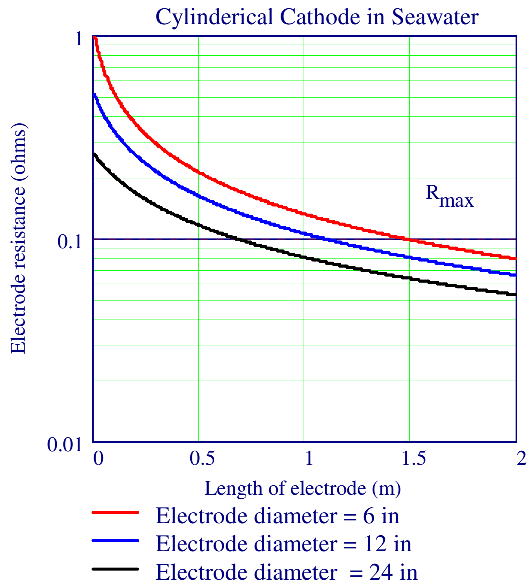

Figure 6 – Cathode Resistance vs. Length of Cylindrical Electrode

The potential, and electric field as a function of distance can now be calculated and the results for a 0.1 m diameter cathode that is 1 m long, are plotted in Figure 7.

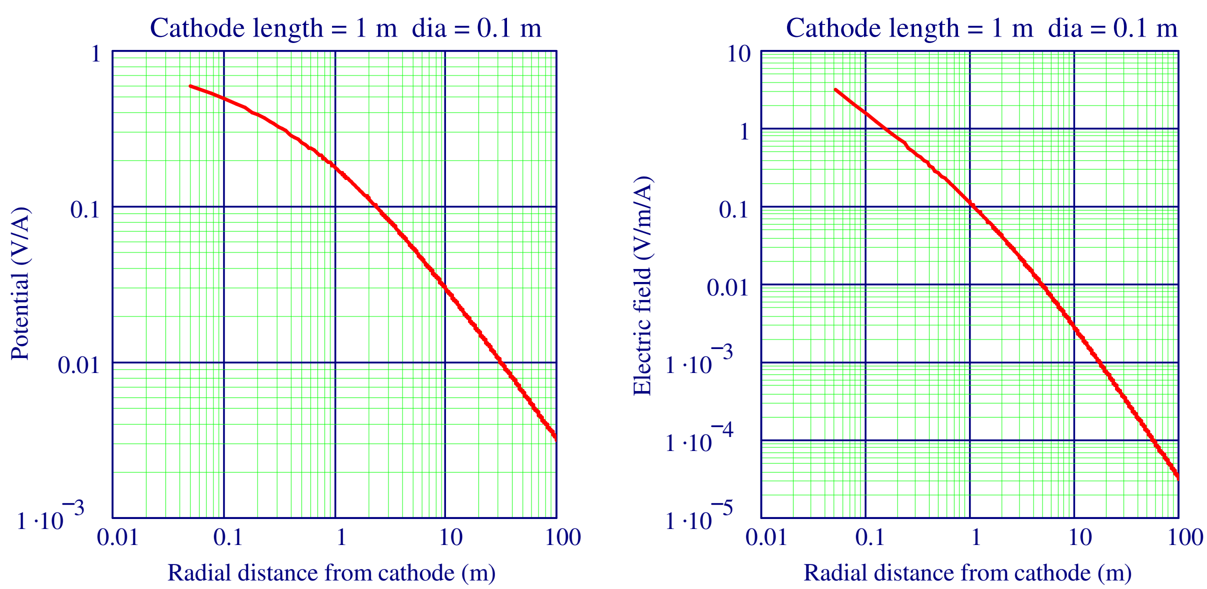

Figure 7 – Potential and Electric Field vs. Distance from Sea Cathode Normalized for 1 A Current

6.3 DC Bipole Cable

The preferred method for subsea DC power transmission is to use a ‘bipole’ cable consisting of two cables; one carrying positive current and the other negative (Figure 8). This has the advantage that high electric fields in the sea associated with sea electrodes are avoided, and a degree of electric and magnetic field cancellation results.

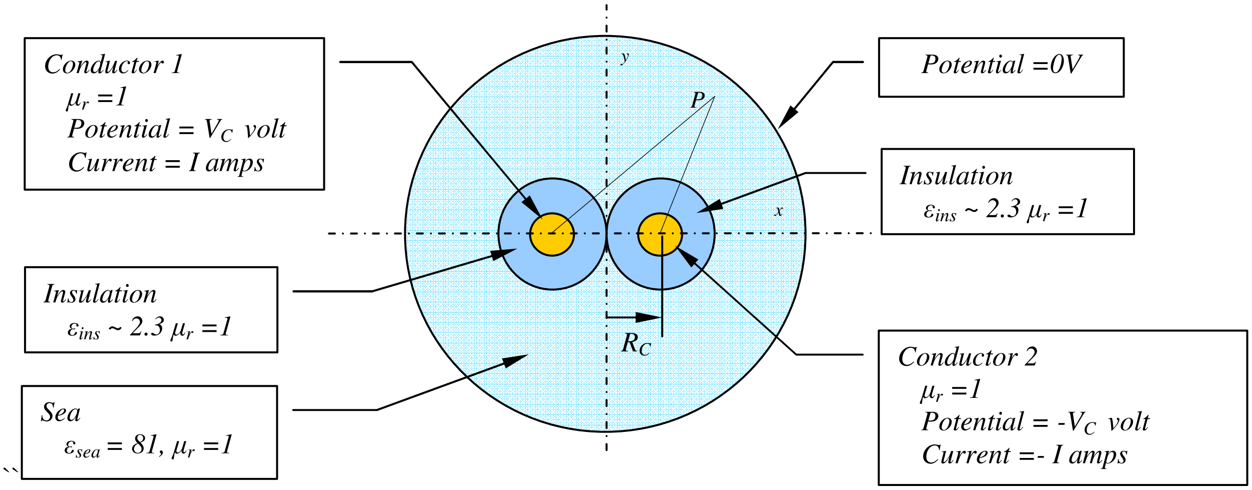

Figure 8 – Unshielded Bipole Cable

The fields surrounding the bipole cable can be determined by superposition of the fields generated by two single cables as follows. Consider the point *P* in Figure 9, which shows the *E* and *B* fields from each individual cable. These vectors can be resolved into the *x* and *y* planes and the resultant *E* and *B* fields derived as a function of the radius *R* and angle θ around the cable. To enable the calculations, the distances R_1, R_2, angles α, and β were determined as functions of *r* and θ by simple trigonometry. It can be shown that:

$$R_1(\theta, r) = \sqrt{R_C^2 + r^2 - 2R_C r\cos(\theta)}$$

$$R_2(\theta, r) = \sqrt{R_C^2 + r^2 + 2R_C r\cos(\theta)}$$

$$\alpha(\theta, r) = \arcsin\left[\frac{r\sin(\theta)}{R_2(\theta, r)}\right]$$

$$\beta(\theta, r) = \pi - \arcsin\left[\frac{r\sin(\theta)}{R_1(\theta, r)}\right]$$

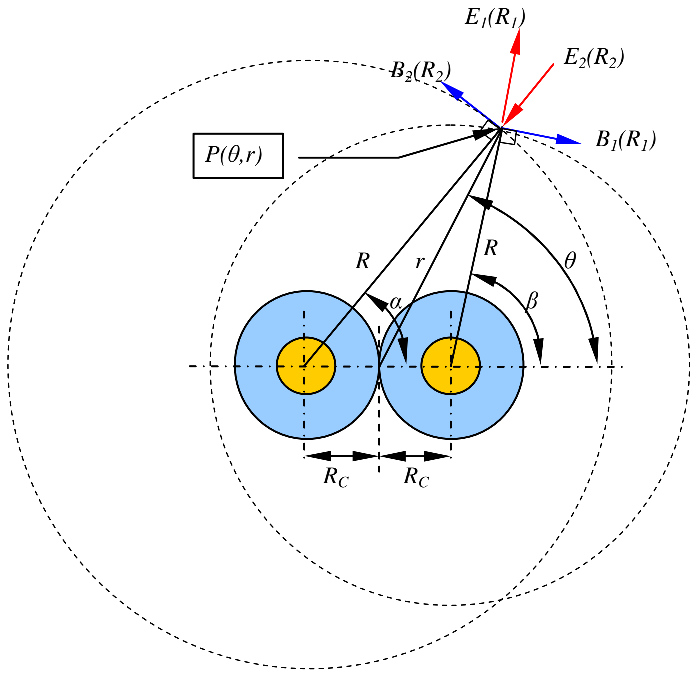

Figure 9 – Components of Electric and Magnetic Fields

From Figure 9, it is apparent that the maximum electric and magnetic fields in the sea occur when $\theta = 0$ or 180°, and the minimum fields occur when $\theta = 90$ and 270° where the fields tend to cancel. The magnetic and electric fields surrounding the cable have been calculated as a function of angle around the bipole, for various radii from the cable axis (Figure 10).

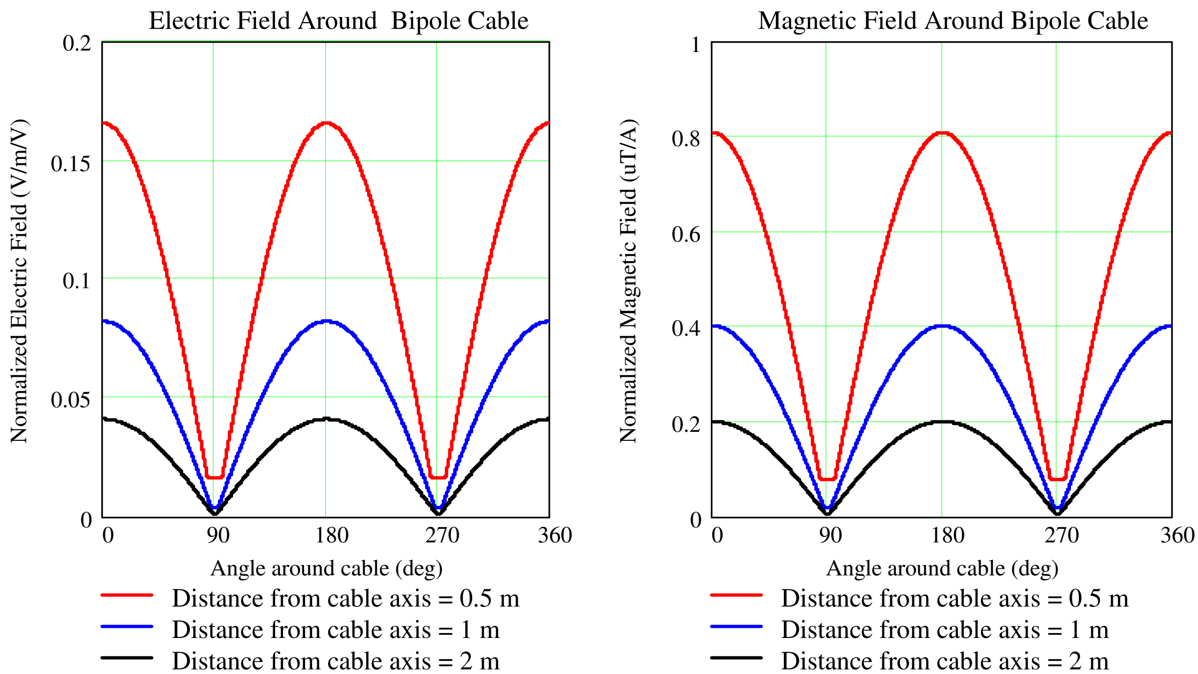

Figure 10 – Normalized E and B Fields around an Ideal Unshielded DC Bipole Cable

Therefore, the *peak* electric field as a function of distance from the cable axis (r) is given by:

$$E_{SEA}(r) = \frac{2V_C C_{INS}}{r \ln\left(\frac{R_O}{R_C}\right).(C_{INS} + C_{SEA})} \quad \text{where } r > R_C \qquad 11)$$

Similarly, the maximum B field can be determined using:

$$B_{SEA}(r) = \frac{I\mu_0\mu_r}{\pi.r} \qquad 12)$$

The normalized electric and magnetic fields as a function of distance form the cable axis are shown in Figure 11, together with the plots for a single DC cable, which demonstrates the degree of field cancellation.

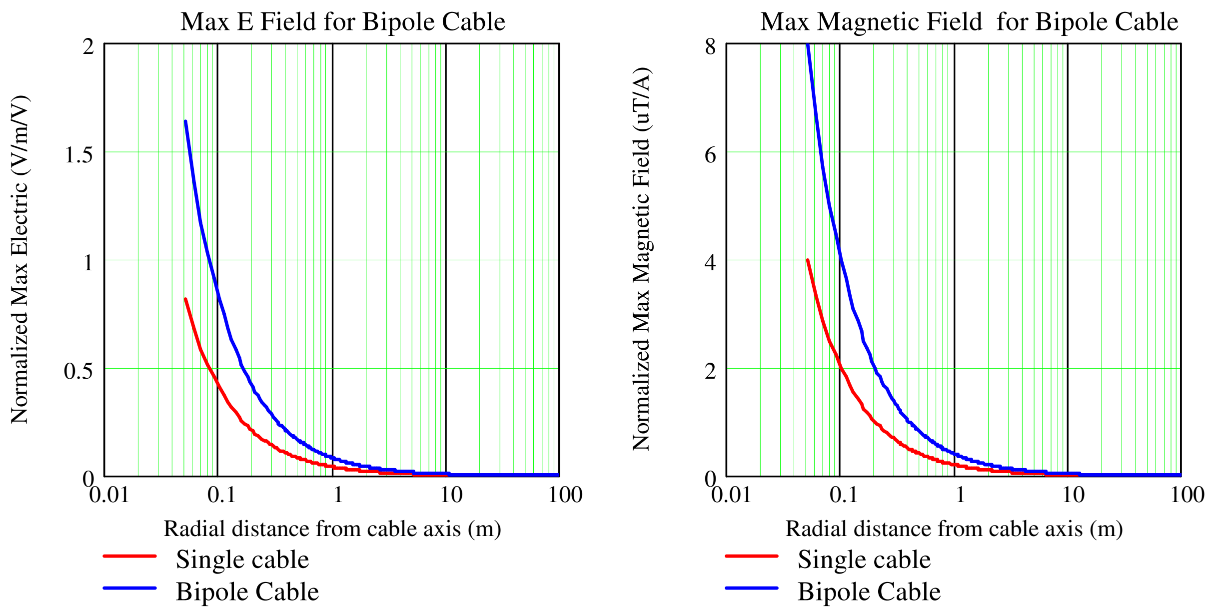

Figure 11 – Maximum E and B Fields vs. Distance from Unshielded DC Bipole Cable

The maximum magnetic field around a bipole DC cable is given by:

$$B_{SEA}(r) = \frac{I\mu_0\mu_r}{\pi . r} + B_{earth} \qquad 13)$$

The maximum magnetic field for a current of 1000 amps is shown in Figure 12.

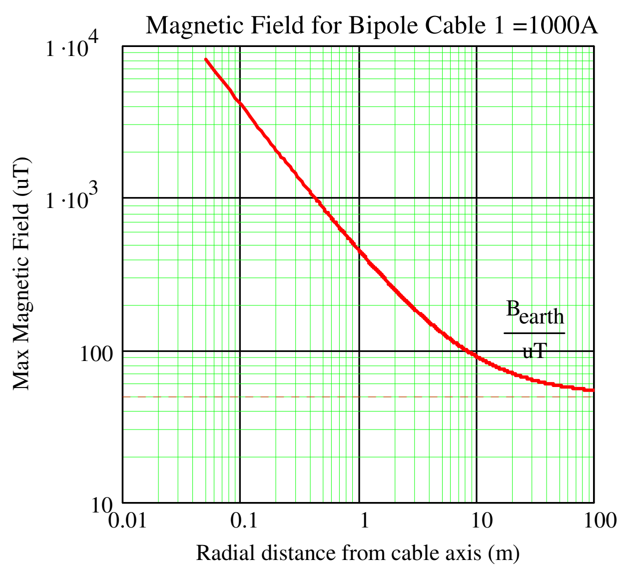

Figure 12 – Maximum Absolute B Field vs. Distance from an Unshielded Bipole Cable
I = 1000 A. Earth's Field assumed to be 50 µT

7. ALTERNATING CURRENT CABLES

The preceding section considered the electromagnetic fields induced in seawater from DC power cables. However, the DC model is not applicable to AC cables, as the impedance of the seawater "return path" must now be considered as alternating fields are propagating into the sea. Further, with a DC power cable in stagnant water, a perfect metallic shield reduces the electric field in the sea to zero, but this is not the case with an AC cable, as there is a time variant (sinusoidal) magnetic field in the seawater, which produces an *induced* electric field in the sea.

7.1 Transmission Line Model

The magnetic and electric fields surrounding an AC power cable can be calculated directly using the concept of a radial transmission line model. Such a transmission line comprises of concentric shells that are thin compared to both the conductor radius and the skin depth (see Appendix C) of a plane wave propagating into the sea (Figure 13).

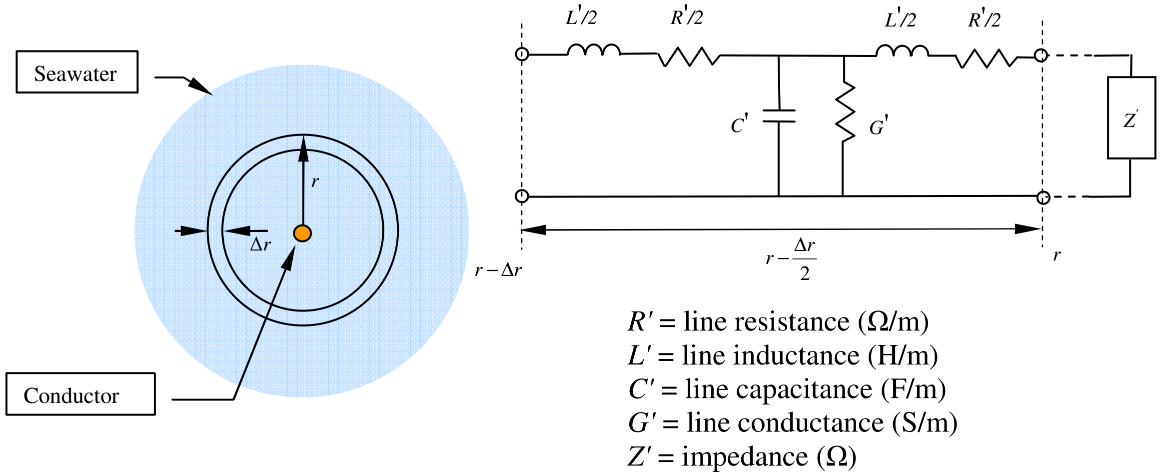

Figure 13 – Radial Transmission Line Concept and Equivalent Circuit

The propagation across *each* shell is defined by near constant parameters at a specific radius. These parameters are the resistance, inductance, conductance, and capacitance of the shell between its inner and outer radii and are used to define the distributed transmission line as seen in Figure 13.

To simplify and provide a realistic boundary condition, the maximum radius for the calculation is selected as 10 times the skin depth over which a plane wave will be attenuated by 10 nepers (-86 dB)

With a 60 Hz power frequency, the skin depth is approximately 32 m in seawater, so the termination impedance can be equated to zero (*i.e.* short circuit) at a radius of approximately 320 m with an error of < 0.005 %.

The input impedance of the line at a specific radius, which relates the voltage (*i.e.* the electric field) to the current (*i.e.* the magnetic field), can now be calculated. If a current of 1 Amp is applied at the line termination, then the current (I_0) required at the input of the line (*i.e.* at the cable surface) to generate the 1 Amp at the termination can be determined. The current at this radius per amp applied at the cable surface, is given by $1/I_0$. The current at the cable surface is the return current in the effective outer conductor of the cable (*i.e.* the sea), and is the same as the current in the inner conductor of the cable. In the practical case, the conductor will be insulated and there may be an external metallic shield or armor wires. In this case, the model comprises of transmission lines in tandem and the line parameters change accordingly.

The required calculations are solved by a Visual Basic macro, previously developed by ENS Consulting, for location of submarine telecommunication cables with a 25 Hz toning signal. The cable construction, power frequency, and distances from the cable are entered into the worksheet, then the program calculates and plots the electric and magnetic fields as a function of radial distance from the cable axis.

7.2 Single Phase AC Cable

Consider an arbitrary single phase shielded cable with the properties detailed in Table 2.

Table 2 – Arbitrary Single Phase Shielded AC Cable

Parameter	Value
Wall thickness of Shield (cm)	0.2
Shield Permeability (steel)	300
Resistivity of shield (μohm.cm)	18
Permittivity of outer jacket	2.3
Wall thickness of outer jacket (cm)	0.5
Conductivity of outer jacket (mho/cm)	1 x10^{-12}
Permittivity of sea	81
Conductivity of sea (mho/cm)	0.04
Cable diameter (cm)	11.4

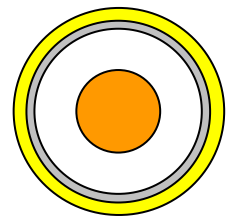

The calculated peak electric and magnetic fields as a function of distance from the cable axis and normalized for a current of 1 amp, are seen in Figure 14.

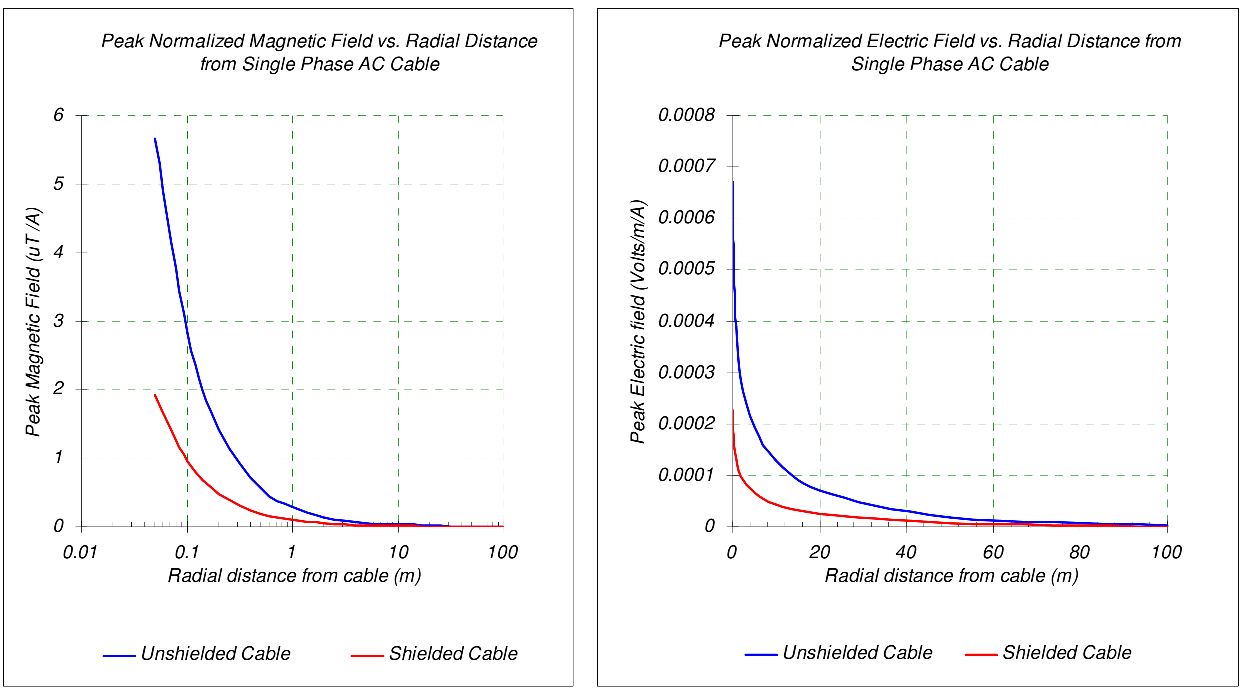

Figure 14 – Normalized Peak E and B Fields around an Arbitrary Single Phase AC cable Frequency = 60 Hz

From Figure 14, it is observed that the shield reduces both the electric and magnetic fields, but the electric field in the sea does not reduce to zero, as occurs with a shielded DC cable, as this electric field is induced by the magnetic field.

The magnetic field is additive to the earth's magnetic field which results in magnetic field "ripple" at the power frequency over the background magnetic field. The peak electric and magnetic fields as a function of distance from a single-phase cable carrying 1000 A (RMS) at 60 Hz are shown in Figure 15.

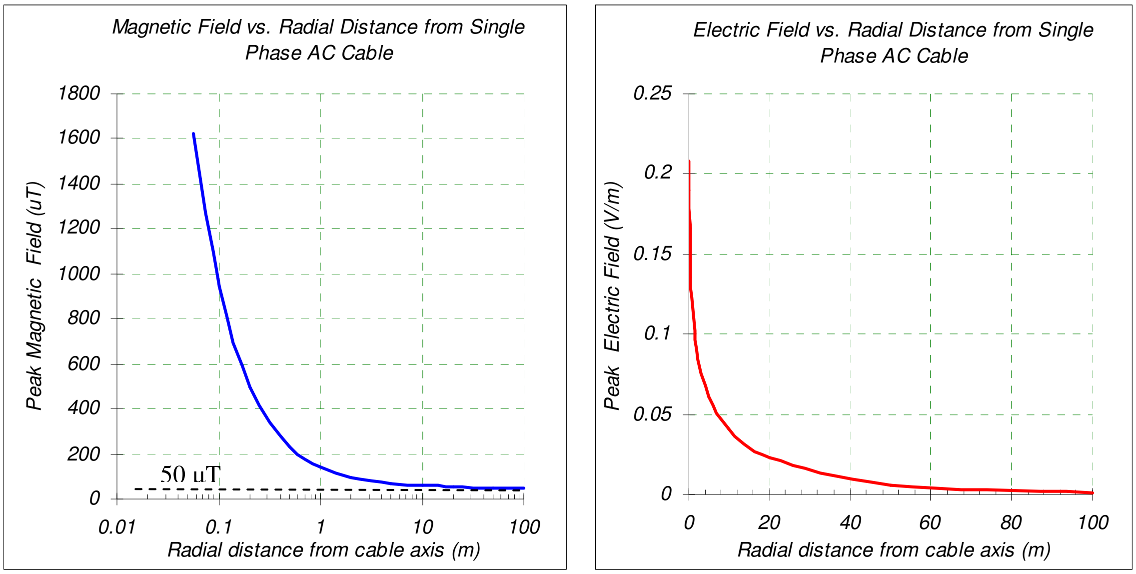

Figure 15 – Peak E and B Fields around an Arbitrary Single Phase AC Cable
Current = 1000 A. Frequency = 60 Hz. Earth's Field = 50 µT (assumed)

To validate the transmission line model, a Finite Element Analysis (FEA) of the shielded cable detailed above was undertaken using Ansoft Maxwell 2D™. The peak electric and magnetic fields predicted by the transmission line model and FEA, as a function of distance from the cable axis, are summarized in Table 3. Good agreement between the two methods is observed, but the FEA model tends to underestimate the electric field and overestimate the magnetic field, if the outer boundary is positioned too close to the cable.

Table 3 – Comparison between FEA and Transmission Line Model Single Phase Cable
Current= 1 A (RMS) Frequency = 60 Hz

Distance from cable axis (m)	*Peak B field by FEA (µT)*	*Peak B field from X-line Model (µT)*	*Peak E field by FEA (V/m)*	*Peak E field from X-line Model (V/m)*
0.1	0.9460	0.95663	0.0001908	0.000202
0.2	0.4800	0.47831	0.0001658	0.000178
0.5	0.1910	0.19128	0.0001325	0.000145
1	0.0966	0.09559	0.0001077	0.000121
2	0.0482	0.04769	0.0000825	0.000096
5	0.0192	0.01881	0.0000495	0.000065
10	0.0096	0.00900	0.0000247	0.000043

The electric and magnetic field at a specific distance from the cable is a function of the power frequency, and these characteristics are shown in Figure 16 for various distances from the cable.

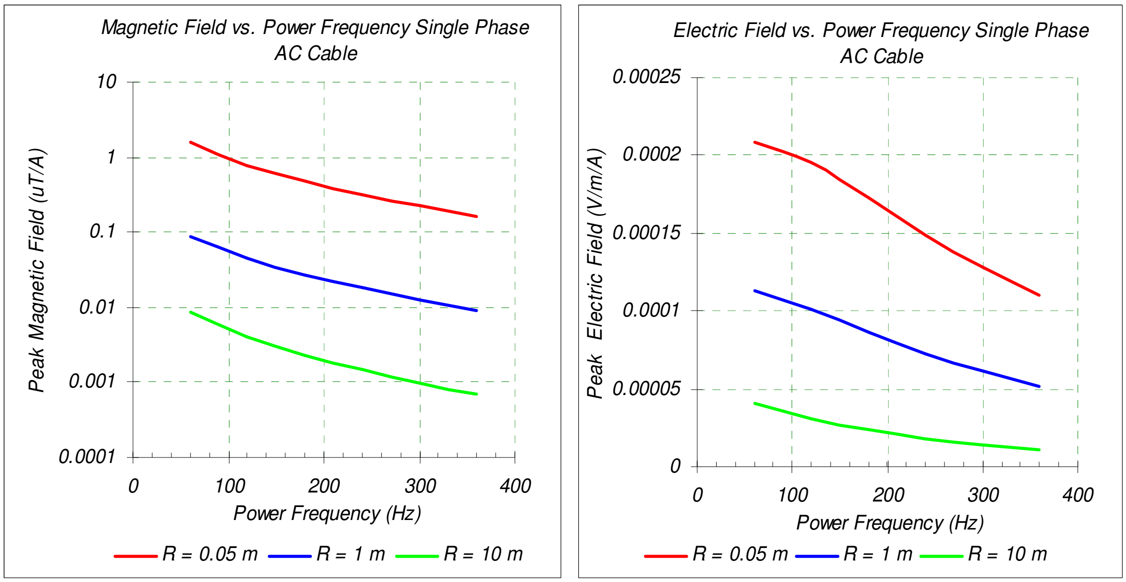

Figure 16 – Normalized E and B Fields vs. Power Frequency for Single Phase Cable

7.3 Individually Shielded Triaxial AC Cable

The most common cable type of subsea 3-phase power transmission is the triaxial, or trefoil cable, where three conductors are laid up in the form of an equilateral triangle.

It is possible to determine the electric and magnetic fields surrounding such a cable by superposition of the fields calculated for a single conductor as previously done for the DC bipole cable. Consider the triaxial cable shown in Figure 17, with each conductor being individually shielded, as specified in Table 2.

In a balanced line the phase currents are 120 degrees out of phase, thus the maximum field rotates around the cable axis with time, shown in Figure 18.

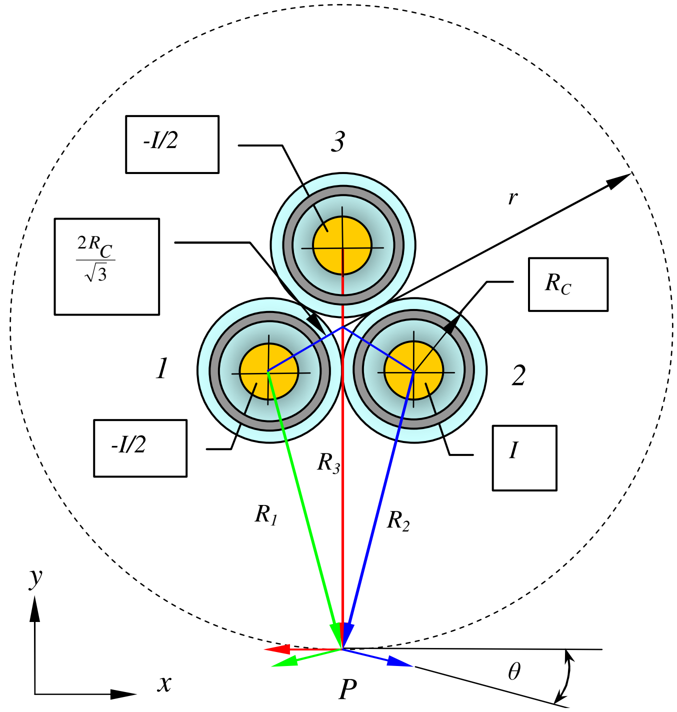

I = Phase current

R_C = radius of cable

R_1, R_2, R_3 = distance from each conductor to the point P

Figure 17 – Vector Diagram for B fields around a Three Phase Triaxial AC Cable Each Phase Individually Shielded

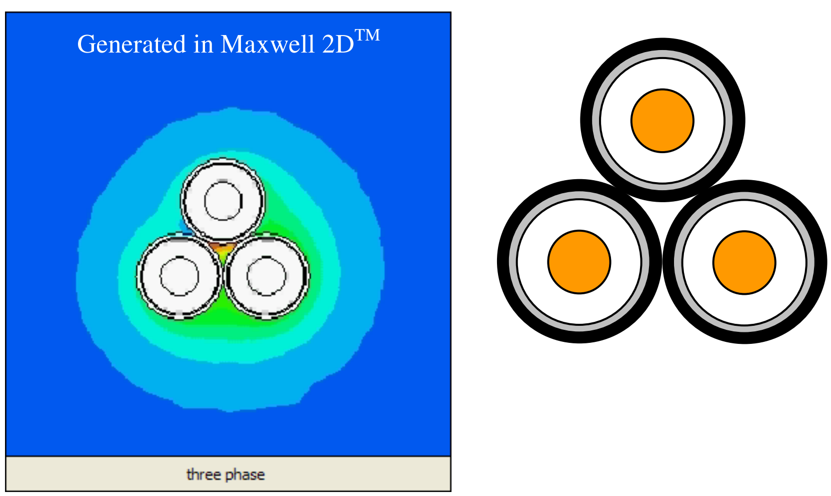

Figure 18 – Magnetic Field Visualization for Individual Shielded Trefoil AC Cable

The values of R_1 and R_2, as shown in Figure 17, were determined using the cosine rule, which yields:

$$R_1(r) = R_2(r) = \sqrt{r^2 + \frac{4R_C^2}{3} - \frac{2R_C r}{\sqrt{3}}}$$

$$R_3(r) = r + \frac{2R_C}{\sqrt{3}}$$

The angle θ in Figure 17, is given by:

$$\theta(r) = \arcsin\left[\frac{R_C}{R_1(r)}\right]$$

Where $\theta(r)$ is in radians

The components of the magnetic field around the 3-phase cable are determined by vector summation of the *B* fields from each conductor.

$$B_y(r) = \frac{3B_{1,2}(r)\sin(\theta(r))}{2}$$

$$B_x(r) = \frac{B_{1,2}(r)\cos(\theta(r)) - B_3(r)}{2}$$

Where $B_{1,2}(r)$ = Magnetic field from conductor 1 or 2 (T)

$B_3(r)$ = Magnetic field from conductor 3 (T)

Similarly, the components of the *E* field were determined to be

$$E_x(r) = \frac{E_{1,2}(r)\sin(\theta(r))}{2}$$

$$E_y(r) = \frac{\cos(\theta(r))\{E_{1,2}(r) - E_3(r)\}}{2}$$

Where $E_{1,2}(r)$ = Electric field from conductor 1 or 2 (V/m)

$E_3(r)$ = Electric field from conductor 3 (V/m)

The resultant fields are given by

$$E(r) = \sqrt{E_x(r) + E_y(r)}$$

$$B(r) = \sqrt{B_x(r) + B_y(r)}$$

Finally, the peak electric and magnetic fields generated by the phase currents are:

$$E_{peak}(r) = k\sqrt{E_x(r) + E_y(r)}$$

$$B_{peak}(r) = k\sqrt{B_x(r) + B_y(r)}$$

Where $k(r) = 2\sqrt{3}$

The maximum fields around the ideal triaxial cable are shown in Figure 19, together with those calculated for the ideal single-phase cable, and it is observed that both the electric and magnetic fields are reduced with the triaxial cable compared to the single-phase cable for distances greater than 0.4 m from the cable axis. However, less than 0.4 m from the axis, the 3-phase cable generates magnetic fields that are higher those produced at the same distance from a single-phase cable carrying the same current.

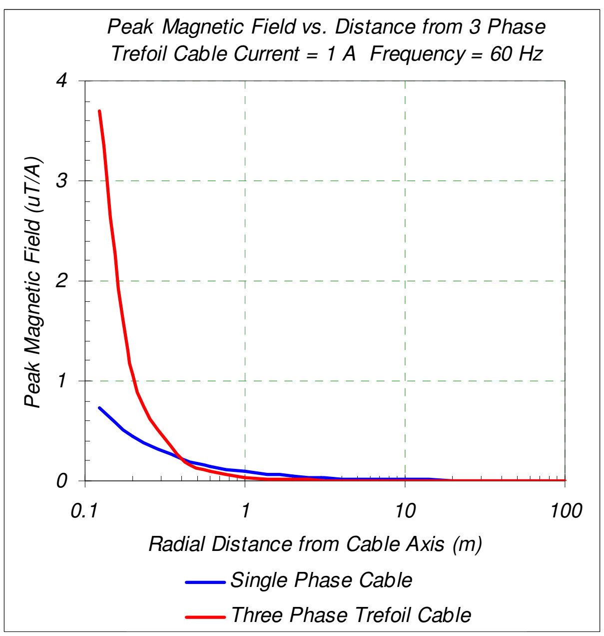

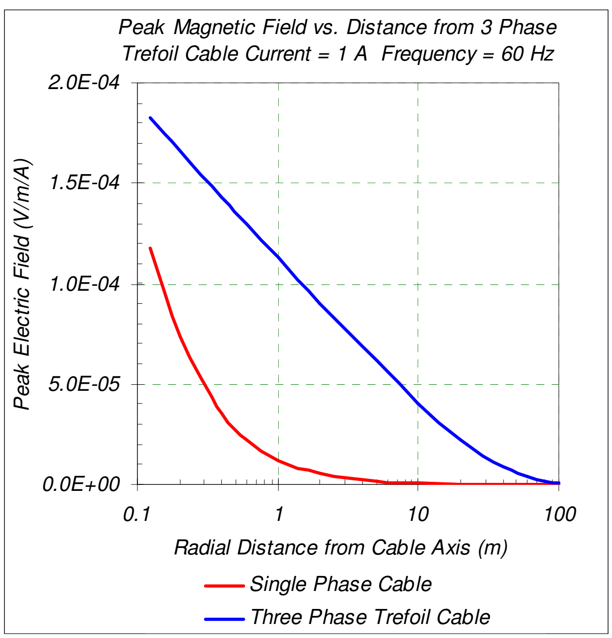

Figure 19 – Electric and Magnetic Fields vs. Distance from Axis of Triaxial cable Each Phase Individually Shielded

To validate the transmission line model for the three phase trefoil cable, the cable was analyzed using Ansoft Maxwell 2D™ and the resulting magnetic potential plot is shown in Figure 20.

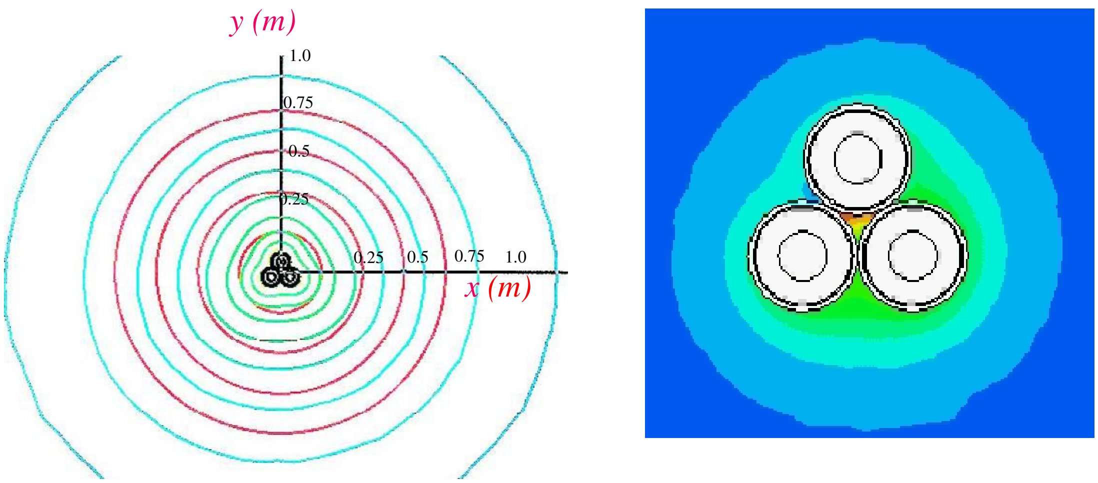

Figure 20 – Magnetic Potential and Field Plots for 3 Phase Trefoil Cable

From Figure 20 it is apparent that the magnetic field becomes near circular for radii greater than 0.5 m from the cable axis, thus close agreement between the TLM and FEA model is expected beyond 0.5 m from the cable. Figure 21 shows the magnetic field along the y-axis in Figure 20, which gives the maximum fields, together with the maximum magnetic fields predicted with the transmission line model.

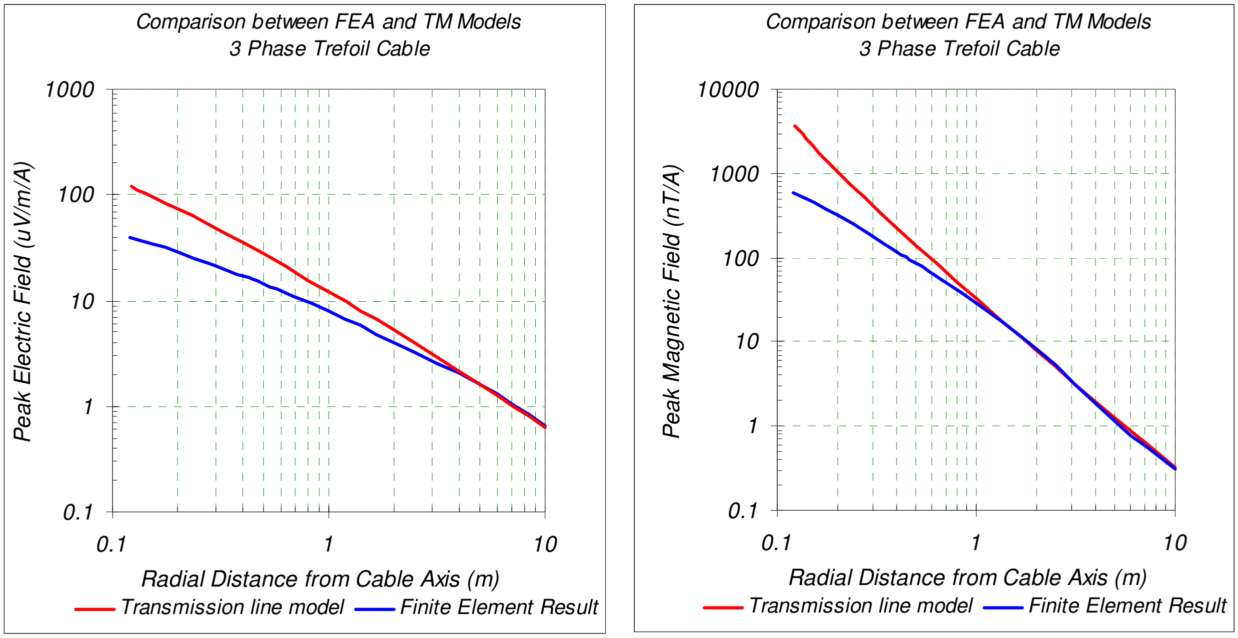

Figure 21 – Normalized E and B Fields by FEA and TLM vs. Distance from Trefoil Cable

Figure 21 demonstrates excellent agreement between the two models for distances greater 1 m from the cable axis and the TLM is conservative in predicting the fields for distances less than 1 m from the cable. The transmission line model for the individually shielded trefoil 3-phase cable is therefore justified.

7.4 Triaxial AC Cable with a Common Outer Shield

Another type of three-phase cable construction is to apply an outer shield, or armor layer, that encompasses all three conductors and examples of this design are shown schematically in Figure 22.

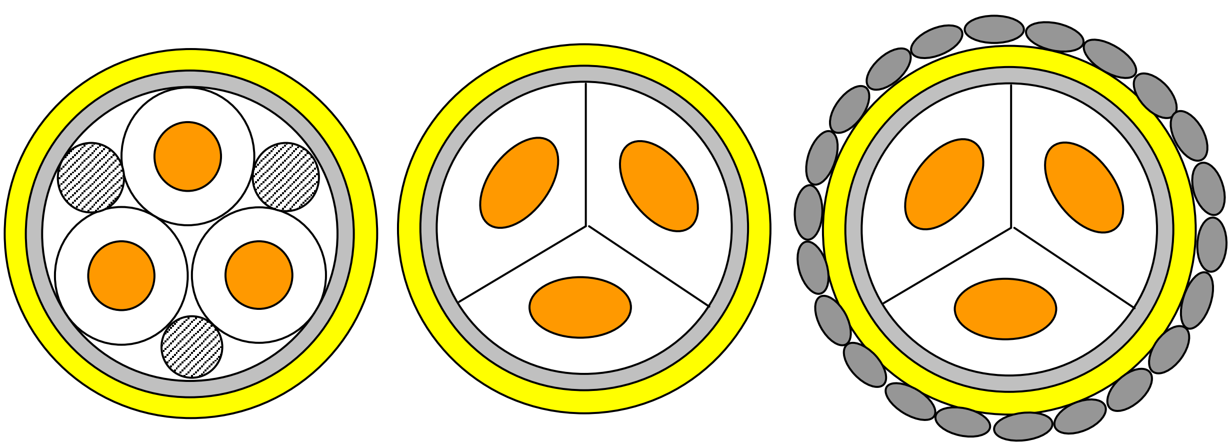

Figure 22 – Schematics of Outer Shielded and Armored Triaxial Cables

The fields external to these cables will be more uniform compared to those surrounding an unshielded trefoil cable (Figure 20) due to the presence of the nominally annular metallic outer conductor (see Figure 23).

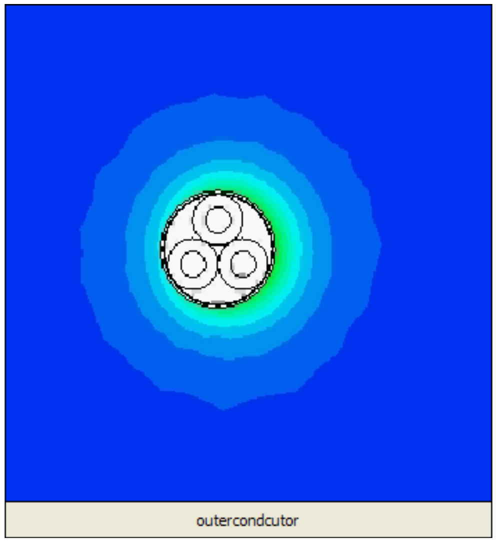

Figure 23 – FEA Visualization of Magnetic Field around Trefoil Cable with Common Outer Armor

To predict the fields around this type of cable using the transmission line model, an effective current must be defined from the phase currents of the three-phase cable as follows:

$$I_{EFF} = \frac{I_{RMS}}{3\sqrt{3}}$$

Where I_{RMS} = RMS phase current of power cable

The normalized fields using the analytic and finite element methods are shown in Figure 24, where excellent correlation of the two methods is again apparent.

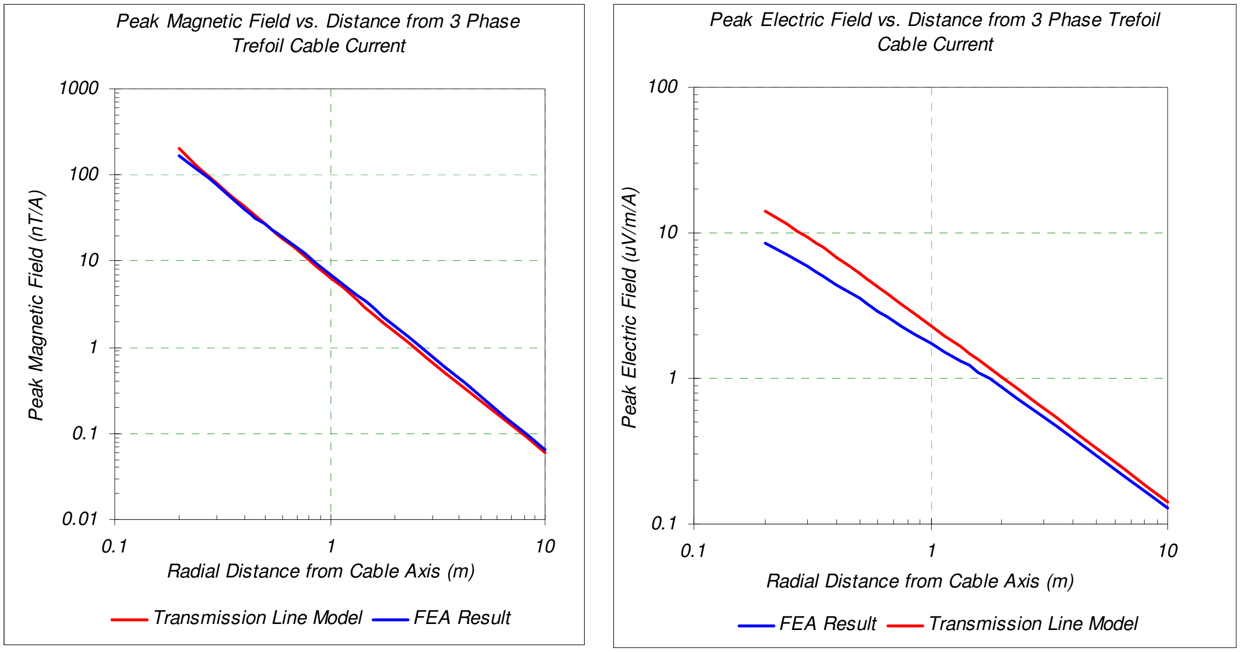

Figure 24 – Normalized Electric and Magnetic Fields vs. Distance from 3 Phase Cable with a Single Outer Shield

8. EFFECT OF CABLE BURIAL

To provide additional protection from external aggression in shallow water, submarine cables are usually buried below the natural seabed to a depth of approximately 1 m. Therefore, the effect of the cable being surrounded by seabed sediments, rather than seawater, on the electric and magnetic fields will now be considered.

The magnetic permeability of the seabed and seawater are approximately unity, as both are non-ferromagnetic, thus burial of the cable into the seabed will not change the magnetic field surrounding the cable.

The electric field external to the cable is dependent on the relative permittivity and conductivity of the medium surrounding the cable.

To determine the effective permittivity of the seabed sediment consider the simplified model where the sand or silt particles are considered as spheres of radius r_s located at the center of cubes of seawater of side r_s, positioned to form a regular lattice as seen in Figure 25.

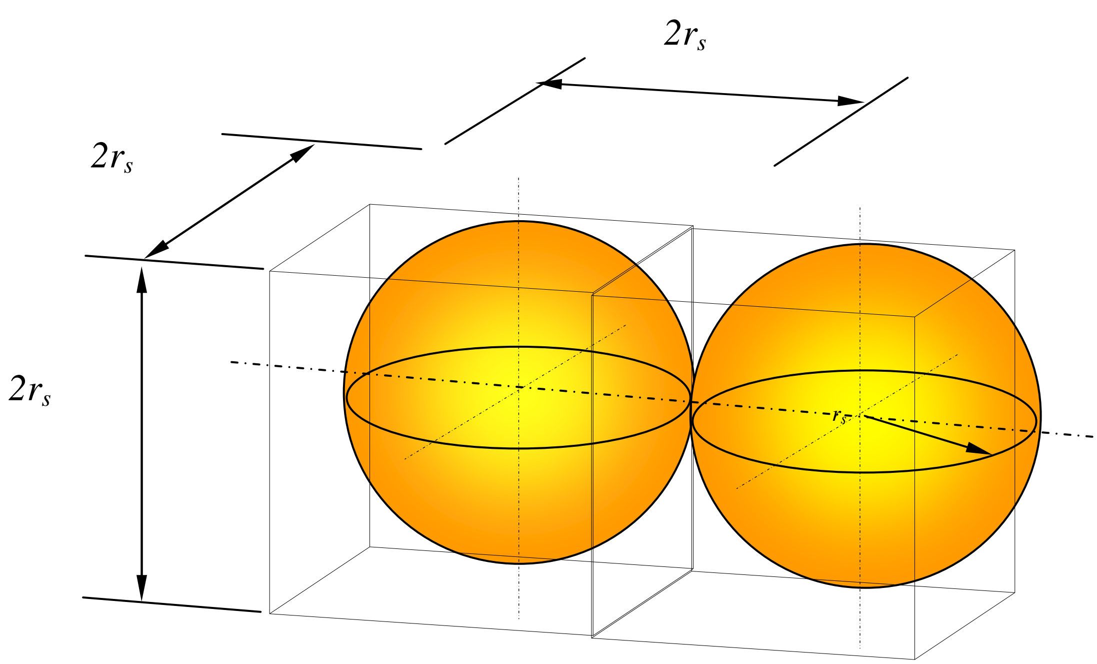

Figure 25 – Model for Determining the Permittivity and Conductivity of Seabed Sediments

From Figure 25, the volume fraction (υ) of the sand particles is given by:

$$\upsilon = \frac{4\pi r_s^{\ 3}}{3(2r_s)^3} = \frac{\pi}{6} = 0.524 \qquad 9)$$

The volume fraction of sand in the seabed sediment can also be defined by:

$$\upsilon = \frac{\rho_{seabed} - \rho_{seawater}}{\rho_{sand} - \rho_{seawater}} \qquad 10)$$

Where ρ_{seabed} = density of seabed (kg/m^3)

$\rho_{seawater}$ = density of seawater (typically 1025 – 1030 kg/m^3)

ρ_{sand} = density of dry sediment (kg/m^3)

The density of silica based seabed sediments is typically 1600 kg/m^3, and the density of silica sand is typically 2100 kg/m^3. Substitution of these values gives a volume fraction of 0.53, which is very similar to that of the regular lattice, and justifies the adoption of the model in Figure 25

Two equations for determining the effective permittivity of a mixture of materials a function of the solid fraction, as arranged in Figure 25, are the Maxwell-Garnett and Bruggeman models (Jylhä and Sihvola, 2007):

$$\varepsilon_{bed}(\upsilon) = \varepsilon_W\left[1 + 3\upsilon\left(\frac{\varepsilon_S - \varepsilon_W}{\varepsilon_S + 2\varepsilon_W - \upsilon(\varepsilon_S - \varepsilon_W)}\right)\right] \quad \text{(Maxwell-Garnett)} \qquad 11)$$

$$\frac{\varepsilon_S - \varepsilon_{bed}}{\varepsilon_S + 2\varepsilon_{bed}}\upsilon + \frac{\varepsilon_W - \varepsilon_{bed}}{\varepsilon_W + 2\varepsilon_{bed}}(1 - \upsilon) = 0 \quad \text{(Bruggeman)} \qquad 12)$$

Where ε_W= Permittivity of seawater (81)

ε_S = Permittivity of solid material (5 for silica)

Similarly, the conductivity of the seabed can be determined using:

$$\sigma(\upsilon) = \sigma_W \left[1 + 3\upsilon \left(\frac{\sigma_S - \sigma_W}{\sigma_S + 2\sigma_W - \upsilon(\sigma_S - \sigma_W)} \right) \right] \tag{13}$$

$$\frac{\sigma_S - \sigma_{bed}}{\sigma_S + 2\sigma_{bed}} \upsilon + \frac{\sigma_W - \sigma_{bed}}{\sigma_W + \sigma_{bed}} (1 - \upsilon) = 0 \tag{14}$$

Where σ_W= Conductivity of seawater (4 S/m)

σ_S = Conductivity of solid material (~ 10^{-10} S/m for silica).

The calculated permittivity and conductivity of the seabed using the two mixing models is shown in Figure 26.

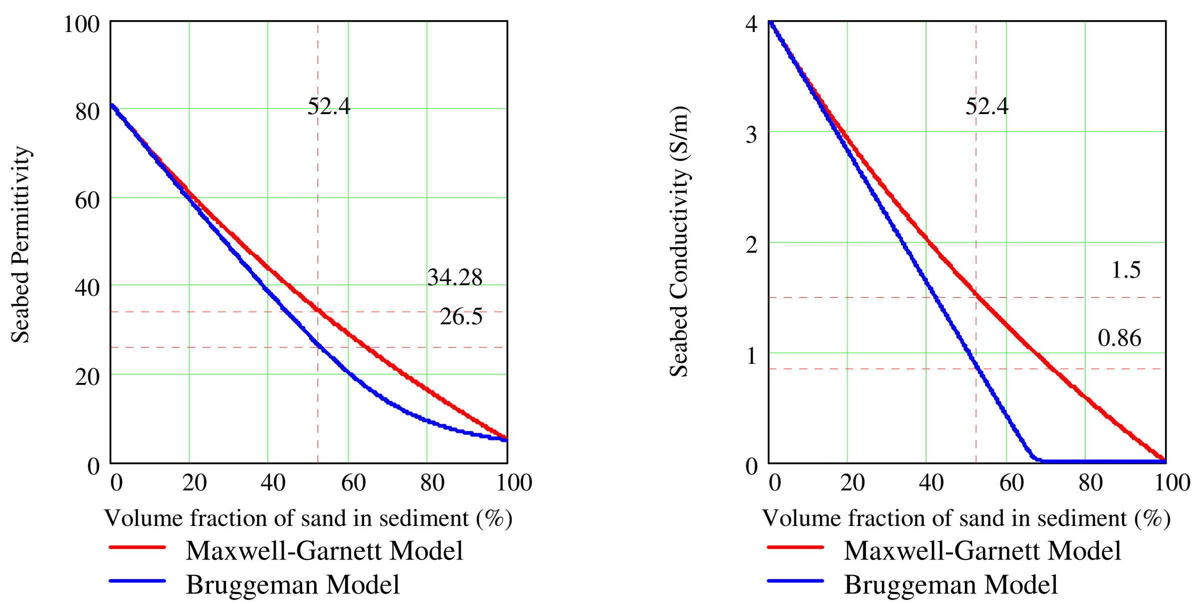

Figure 26 – Effective Permittivity and Conductivity of the Sea Bed

In practice, the actual value of permittivity or conductivity will lay between those predicted by the two models. Therefore, for a solid fraction of 0.524, the effective conductivity is expected to be between 0.86 and 1.5 S/m, and the permittivity will be between 26 and 34.

Consider a single-phase cable buried below the seabed as shown in the simplified model in Figure 27.

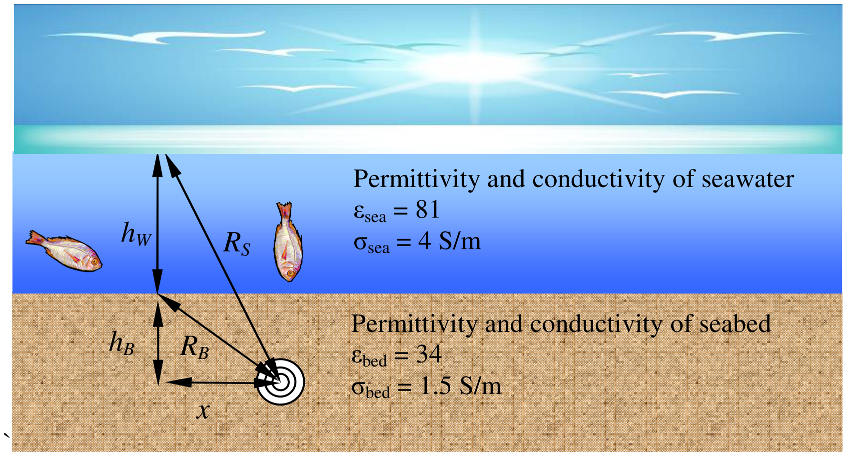

Figure 27 – Cable Burial Model

The radial distances from the cable to the seabed and the surface of the sea as a function of distance from the cable in the x direction are given by:

$$R_B(x) = \sqrt{x^2 + h_B{}^2} \quad \text{and} \quad R_S(x) = \sqrt{x^2 + (h_B + h_W)^2} \tag{15}$$

The highest fields occur at the interface with the seabed, due to the lower permittivity of the seabed sediments. This is demonstrated in Figure 28, which shows the fields at the seabed and sea surface as a function of the perpendicular distance (x) from the cable for a burial depth of 1m and a water depth of 50 m.

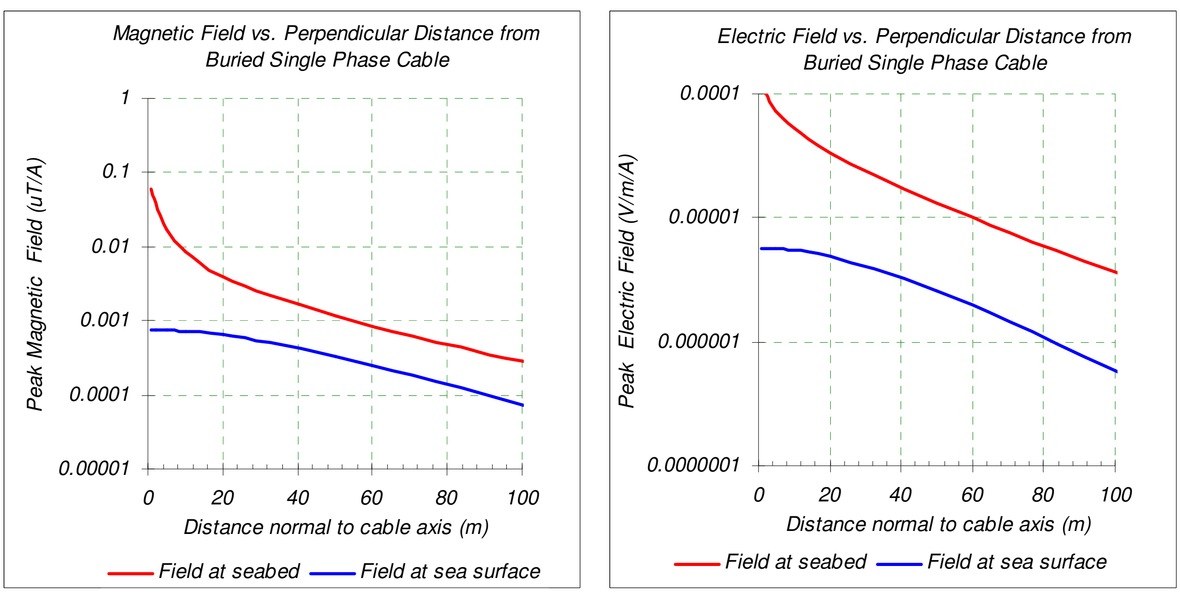

Figure 28 – Normalized Magnetic and Electric fields for a Buried Single Phase Cable
Water Depth = 50 m. Burial depth = 1 m. $\varepsilon_{sea} = 81$ $\varepsilon_{seabed} = 34$ $\sigma_{sea} = 4$ S/m $\sigma_{seabed} = 1$ S/m

9. COMPARISON OF PREDICTED FIELDS WITH MEASUREMENT

The COWRIE report detailed the magnetic and electric field measurements made on two 3-phase power cables, which cross the River Clwyd near the Foryd Bridge (see Figure 29).

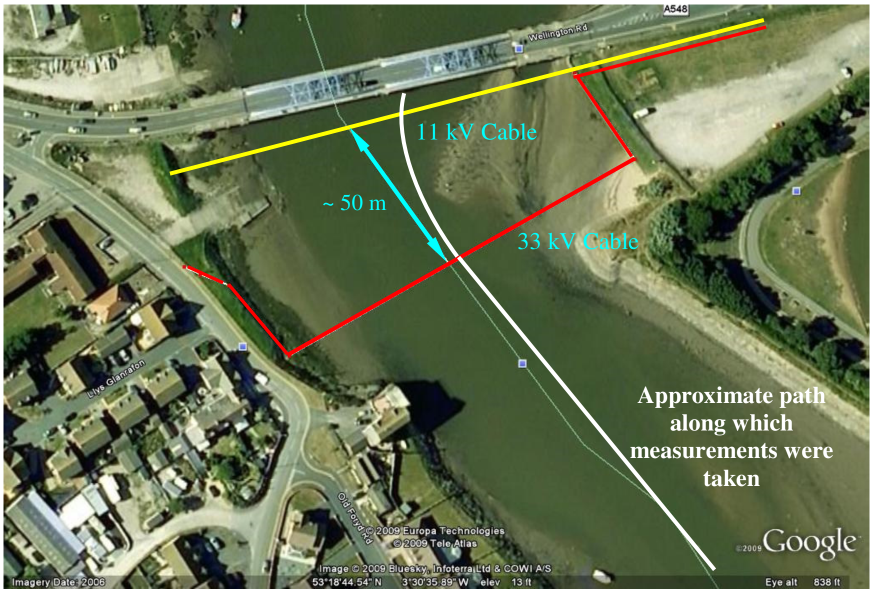

Figure 29 – Location of Power Cables across River Clwyd

It was found that the electric field was >70 µV/m irrespective of where the measurement was made, but no reason for this was presented in the report. If the river flow was 3 knots, which is certainly plausible, a 'background' electric field of >70 µV/m would be produced by magneto-hydrodynamic generation, which could account for the electric field being >70 µV/m.

The COWRIE report did not detail the cable construction particularly well, but did reference the 33 kV cable and 11 kV cables as conforming to BS 6480 and EATS 09-12 respectively. These specifications are given in Appendix D for reference, and have been used to define the cable dimensions required for the analysis.

The cables were reported as buried in the riverbed by approximately 1 m, and the sensors were deployed approximately 1.5 m below the water surface. Unfortunately, the water depth was not reported, but literature surveys indicate a water depth of two or three meters in this location (US Navy, 1917). The predicted performance, using the transmission line model described herein, and the actual measurements for the two cables are shown in Figure 30, which shows very good correlation between theory and reality.

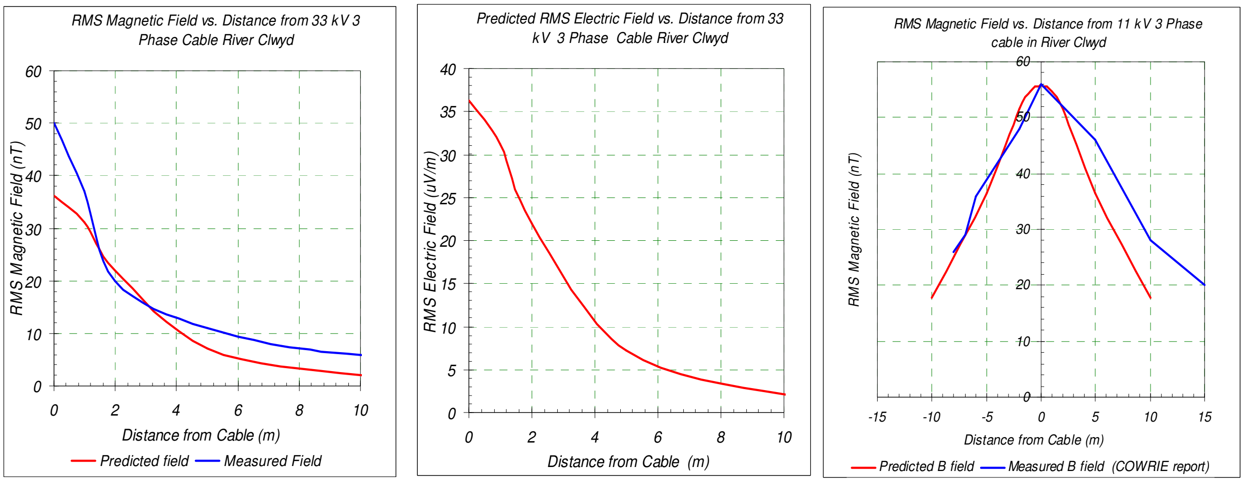

Figure 30 – Predicted and Actual Field Measurements on 33 and 11 kV 3 Phase Cable across the River Clwyd

10. CONCLUSIONS

This report has presented models for predicting the electromagnetic fields produced by DC monopole and bipole power cables that are based on fundamental physical laws.

A transmission line model was developed to enable the electromagnetic fields surrounding an AC cable as a function of distance from the cable, to be quickly and accurately determined from the cable construction, the power frequency, and phase current. The model was developed for both single phase and trefoil three phase cables, with either individual phase shields, or with a single shield that encompasses all three phases. The model has been verified using Finite Element Analysis, and has accurately predicted the fields recorded during 2002, from a pair of 3 phase cables that cross the River Clwyd. It is concluded that the transmission line model will reasonably predict the fields generated around specific cable designs being considered for subsea power transmission.

This work has also shown that if sea trials are to be undertaken to measure the fields adjacent to power cables, the actual location of the sensors relative to the cable must be known as the fields decrease rapidly in close proximity to the cables. Caution should be exercised when extrapolating these analytical results for a specific site; simplifying assumptions made for the homogeneity of the surrounding medium (e.g. seawater or underlying geology) may affect the accuracy as one moves away from the vicinity of the electrical cable source unless such features are incorporated into the calculations.

The normalized magneto-hydrodynamic electric field produced when seawater moves through the earth's magnetic field is approximately 0.515 V/m/knot/T, and will change 'polarity' with flow reversal (i.e. tidal effects). This field is additive to the electric field produced by the current flow in the cable, therefore, when developing systems for measuring the E-field adjacent to a power cable, methods for accounting for this 'background' field must be defined.

APPENDIX A – GLOSSARY OF SYMBOLS

$\alpha, \beta, \theta, \phi$	Angle	radians
a	Current loop radius	m
A	Magnetic vector potential	$Wb{\cdot}m^{-1}$ or $T{\cdot}m$
B	Magnetic Field	Tesla
β'	Phase constant	$radian{\cdot}sec^{-1}$
C',C	Transmission line capacitance	$F{\cdot}m^{-1}$
dA	Area of current loop	m^2
δ	Skin depth	m
E	Electric field	$V{\cdot}m^{-1}$
ε_0	Permittivity of free space	8.66×10^{-12} $F{\cdot}m^{-1}$
ε_r	Relative permittivity	
f	Power frequency	Hz
G'	Transmission line conductance	$S{\cdot}m^{-1}$
h	Depth	m
I	Current	Amperes
l	Length	m
L'	Transmission line inductance	$H{\cdot}m^{-1}$
λ	wavelength	m
μ_0	Permeability of free space	$4\pi \times 10^{-7}$ $N{\cdot}Amp^{-2}$
μ_r	Relative permeability	
v_p	Phase velocity	$m{\cdot}sec^{-1}$
v	Sea water flow velocity	$m{\cdot}sec^{-1}$
Q	Charge	coulomb
q	Charge/unit length	$coulomb{\cdot}m^{-1}$

r	Radial distance	m
R'	Transmission line resistance	$\Omega \cdot m^{-1}$
R_1, R_2, R, R_C	Radii	m
ρ	Resistivity	$\Omega \cdot m$
σ	Conductivity	$S \cdot m^{-1}$
$\hat{\theta}$	Unit vector in θ	
V	Potential	volts
υ	Volume fraction	
ω	angular frequency	$radians \cdot sec^{-1}$
x, y, z	Cartesian coordinates	m
Z	Impedance	Ω
Z'	Transmission line impedance	Ω
$\hat{z}$	Unit vector in z	

APPENDIX B – ACRONYMS

ASW	anti-submarine warfare
B-field	magnetic field
BWEA	British Wind Energy Association
CA	California
CGS	centimeter-gram-second
CMACS	Centre for Marine and Coastal Studies
COWRIE	Collaborative Offshore Wind Research Into The Environment
DECC	Department for Energy and Climate Change
DoI	Department of Interior
EA	Environmental Assessment
E-field	electric field
EIS	Environmental Impact Statement
EM	electromagnetic
EMF	electromagnetic field
FEA	Finite Element Analysis
Hz	Hertz, cycles per second
MHD	magneto hydrodynamic
MHz	megahertz
MKS	meter-kilogram-second
MMS	Minerals Management Service
ODFW	Oregon Department of Fish and Wildlife
OPT	Ocean Power Technologies
OR	Oregon
OWET	Oregon Wave Energy Trust
PSD	Power spectral density
RMS	Root Mean Square
SI	International System of Units
SIO	Scripps Institute of Oceanography
THz	terahertz
UK	United Kingdom
WA	Washington

APPENDIX C – SKIN DEPTH

The skin depth describes the extent that an electromagnetic wave penetrates into a material, and is defined as the distance at which the amplitude of the incident wave is attenuated to 1/*e* of the initial value. A mirror is an example of this effect, where the light is reflected from the surface of a metalized coating and energy is also absorbed into the material. The incident wavelength (energy) propagates into the metallic coating, decaying exponentially with penetration distance. The visible spectrum ranges from 400 to 800 THz, and the skin depth for silver varies from 0.07 to 0.1 nm over this frequency band. Therefore, the E and B fields of the incident wavelengths, which penetrate into the silver coating, decay to near zero within a nanometer of the surface.

Similarly, if an AC current is passed through a conductor, the current density will be highest at the conductor surface, and decay with distance toward the center of the conductor. The skin depth of copper at 60 Hz is approximately 8.5 mm, so ~63 % of the current flows within 8.5 mm of the conductor surface. Therefore, a copper bus bar with a radius > 10 mm is essentially 'wasting' copper.

The generalized equation for the skin depth as a function of frequency ($\delta(f)$) can be derived from Maxwell's (1873) equations, and is:

$$\delta(f) = \frac{1}{\omega(f)}\sqrt{\frac{2}{\mu_r \mu_0 \varepsilon_r \varepsilon_0}}\left[\sqrt{1+\left(\frac{\sigma}{\omega(f)\varepsilon_r \varepsilon_0}\right)^2}-1\right]^{-\frac{1}{2}} \qquad \text{A1)}$$

Where $\omega(f)$ = angular frequency = $2\pi f$

μ_r = relative permeability of material

μ_0 = permeability of free space ($4\pi \times 10^{-7}$ N·Amp^{-2})

ε_r = relative permittivity of material

ε_0 = permittivity of free space (8.854×10^{-12} Farad/m)

σ = conductivity of material (S/m)

If $\frac{\sigma}{\omega(f)\varepsilon_r \varepsilon_0} >> 1$, then equation A1) reduces to:

$$\delta(f) = \sqrt{\frac{2}{\omega(f)\mu_r\mu_0\sigma}} \qquad \text{A2)}$$

Equation A2) is the used to calculate the skin depth as a function of frequency for good conductors such as metals or seawater. However, as the frequency increases, equation A2) will no longer be valid, and the high frequency approximation must then be used, which is:

$$\delta = \frac{2}{\sigma}\sqrt{\frac{\varepsilon_r\varepsilon_0}{\mu_r\mu_0}} \qquad \text{A3)}$$

It should be noted that the high frequency approximation is independent of frequency, and the maximum frequency for which the *low* frequency approximation is valid is given by:

$$f_{\max} = \frac{\sigma}{4\pi\varepsilon_r\varepsilon_0} \qquad \text{A4)}$$

Using equation A4), the low frequency approximation is valid for copper for frequencies up to approximately 5 x 10^5 THz, whereas with sea water, the low frequency approximation is valid up to approximately 400 MHz.

The skin depth vs. frequency for copper, seawater, and freshwater using Equation A1, are shown in Figure A1, which is also annotated with the approximation regimes given above.

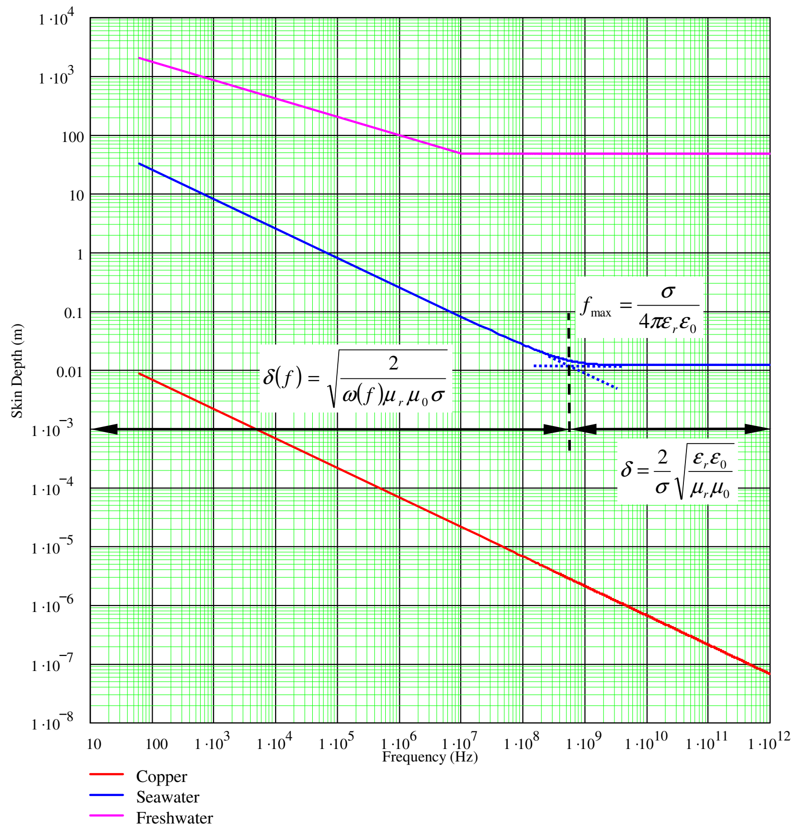

Figure A-1 – Skin depth vs. Frequency for Various Materials

The power frequency will probably be 50 or 60 Hz, justifying the low frequency approximation, which was used in the transmission line model for predicting the electric and magnetic fields surrounding an AC submarine power cable.

The skin depth in seawater at 60 Hz is ~ 32.5 m, and at this distance from the cable, the electric and magnetic fields will have attenuated by 1 neper (8.6 dB) from their values at the cable surface.

APPENDIX D – CABLE TYPES USED IN COWRIE REPORT

General Cable

PAPER LEAD 3C
19/33kV
COPPER
H Type

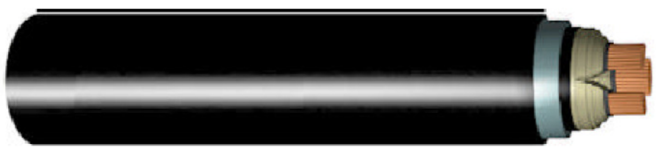

APPLICATION

In urban networks for primary supply to underground residential distribution substations. Main feeders to commercial and industrial projects. The lead sheath provides an earth fault capacity adequate for many installations although it is fixed, and usually less than the equivalent XLPE copper wire screened cable. Each core is screened with metallised paper to distribute electrical stresses evenly through the paper insulation.

STANDARD	AS 1026:1992 BS 6480:1988
VOLTAGE	19000/33000V
CONDUCTOR	Shaped Compacted Annealed Copper
INSULATION	Mass Impregnated (Non Draining) Paper
SHEATH	PVC, 4V-75 or MDPE
MAX. OPERATING TEMP.	65 °C

Conductor		Overall Diameter		Approximate Mass		Minimum Bending Radius	
mm^2	(No./mm)	Minimum mm	Maximum mm	MDPE kg/km	PVC kg/km	Installed mm	During Installation mm
50	19 strands	60.2	64.5	8900	9000	1160	1930
70	19 strands	62.5	66.9	10000	10200	1200	2010
95	19 strands	65.0	69.3	11300	11500	1250	2080
120	19 strands	67.7	72.2	12800	13000	1300	2160
150	19 strands	68.9	73.3	13900	14200	1320	2200
185	37 strands	72.6	77.0	16000	16200	1390	2310
240	37 strands	77.0	81.6	18600	19000	1470	2450
300	37 strands	81.2	85.9	21400	21700	1550	2580

Lengths and packing can be supplied to customer's requirements.
For glanding details, contact your local service centre.
Bending radii to BS6480

	CURRENT RATING (a)		ELECTRICAL CHARACTERISTICS						
Nominal Area	Buried Direct 	Buried In Ducts 	Max. DC Resistance @ 20°C	Max. AC Resistance @ 65°C	Inductance	Equivalent Star Reactance	Capacitance	3 Phase Voltage Drop	1 Sec Fault Rating (b) 3 Phase Symmetrical
mm^2	A	A	ohm/km	ohm/km	mH/km	ohm/km	µF/km	mV/A.m	kA
50	169	148	0.387	0.456	0.403	0.127	0.230	0.82	5.7
70	204	178	0.268	0.316	0.350	0.110	0.280	0.58	7.9
95	242	211	0.193	0.235	0.328	0.103	0.318	0.44	10.7
120	275	240	0.153	0.181	0.315	0.099	0.346	0.36	13.6
150	311	271	0.124	0.147	0.301	0.095	0.384	0.30	16.9
185	349	305	0.099	0.118	0.292	0.092	0.418	0.26	20.9
240	401	350	0.075	0.090	0.280	0.088	0.464	0.22	27.1
300	451	393	0.060	0.073	0.272	0.085	0.507	0.19	33.9

(a)- Based on 65°C maximum conductor temperature, burial depth of 0.8m, soil temperature of 15°C and thermal resistivity of 1.2°Cm/W.
(b)- For fault durations other than one second, divide the appropriate given value by the square root of the required time (in seconds).
Conductor fault ratings are based on an initial temperature of 65°C and a final temperature of 150°C.

CONDUCTOR			LEAD ALLOY SHEATH				
Nominal Area	Nominal Depth	Min.Insulation Between Conductor and Sheath	Minimum Thickness	Diameter over sheath		Nominal Area	1 Sec Fault Rating (c)
				Minimum	Maximum		
mm^2	mm	mm	mm	mm	mm	mm^2	kA
50	8.1	7.3	2.2	56.0	59.8	403	12.2
70	7.4	7.3	2.3	58.1	62.1	438	13.3
95	8.7	7.1	2.4	60.4	64.3	474	14.4
120	9.7	7.1	2.5	62.9	66.9	514	15.6
150	10.7	6.8	2.6	63.9	67.8	541	16.4
185	12.1	6.8	2.7	67.4	71.3	592	18.0
240	13.8	6.8	2.8	71.6	75.6	653	19.8
300	15.5	6.8	2.9	75.6	79.7	714	21.6

(c)- For fault durations other than one second, divide the appropriate given value by the square root of the required time (in seconds).
Sheath fault ratings are based on an initial temperature of 55°C and a final temperature of 250°C.

UTILITY CABLES

MEDIUM VOLTAGE

6350/11000V

EATS 09-12 (11kV Screened) PICAS Cable

CABLE CHARACTERISTICS

Bending radius
R=12D

WWW.CABLEJOINTS.CO.UK
THORNE & DERRICK UK
TEL 0044 191 490 1547 FAX 0044 477 5371
TEL 0044 117 977 4647 FAX 0044 977 5582
WWW.THORNEANDDERRICK.CO.UK

CABLE DESCRIPTION

1.CONDUCTOR
Compact sector shaped stranded aluminium conductor complying with BS6360 Class 2.

2.CONDUCTOR SCREEN
Semi-conducting carbon paper tapes.

3.INSULATION
Layers of paper tapes applied helically and mass impregnated with non-draining insulating compound (MIND)

5.INSULATION SCREEN
Semi-conducting carbon tapes applied in combination with metallised paper tapes over the core insulation. Core identification, Outer carbon papers printed with white numbers 1, 2 and 3.

4 & 6.LAYING UP
Three cores laid up with paper fillers and bound with copper woven fabric tape.

7.ALUMINIUM SHEATH
Extruded corrugated aluminium sheath with bitumen coating.

8.CABLE SERVING
Extruded red polyvinyl chloride (PVC) is supplied as standard.

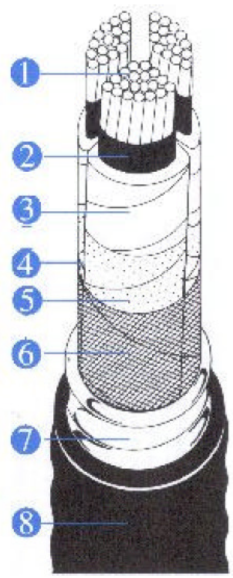

UTILITY CABLES

MEDIUM VOLTAGE

6350/11000V

EATS 09-12 (11kV Screened) PICAS Cable

Constructional Data

Nominal cross-sectional area mm²	Minimum thickness of insulation between conductor and screen mm	Approximate thickness of aluminium sheath mm	Minimum average thickness of oversheath mm	Approximate diameter overall mm
95	2.8	1.2	2.5	49.0
185	2.8	1.6	2.8	60.7
300	2.8	2.0	3.2	72.5

Installation Data

Nominal cross-sectional area mm²	Approximate cable weight Kg/m	Minimum bending radius mm	Nominal internal diameter of ducts mm
95	3.4	600	100
185	5.2	750	100
300	7.5	900	125

Electrical Data

Nominal cross-sectional area mm²	Maximum DC resistance of phase conductors at 20°C Ohms/km	Maximum AC resistance of conductors at 65°C Ohms/km	Approximate reactance at 50Hz Ohms/km	Approximate capacitance µF/km
95	0.320	0.384	0.087	0.600
185	0.164	0.198	0.081	0.810
300	0.100	0.122	0.077	0.100

Ratings Data

Nominal cross-sectional area mm²	Current Ratings		
	Laid direct in ground Amps	Drawn into ducts Amps	Laid in air Amps
95	205	170	200
185	295	250	305
300	380	325	410

Current Rating Conditions:

Ground Temperature	15°C
Depth of Burial	0.8m
Ambient temperature (air)	25°c
Thermal Resistance of Soil	1.2°C m/W

APPENDIX E – BIBLIOGRAPHY

(1) Centre for Marine and Coastal Studies (CMACS). (2003). *A Baseline Assessment of Electromagnetic Fields Generated by Offshore Windfarm Cables* (COWRIE Technical Report EMF 01-2002 66). Birkenhead, England, UK: downloaded from http://www.offshorewind.co.uk/Assets/COWRIE_EMF_Research_Report.pdf

(2) Ida, Nathan. (2004). *Engineering Electromagnetics*, (2nd ed.). New York, NY: Springer, pp. 1124-1129.

(3) Jylhä, Liisi, Ari Sihvola. (2007). "Differential Equations for the Effective Permittivity of Random Mixture of Spheres." EMTS 2007 - International URSI Commission B - Electromagnetic Theory Symposium, Ottawa, ON, Canada, downloaded from http://www.ursi.org/B/EMTS_2007/R10-24/1-Jylha026.pdf

(4) Maxwell, James C. (1873). *A Treatise on Electricity and Magnetism*, Vol. 1. London, England: Macmillan and Co. downloaded from http://www.archive.org/details/electricandmagne01maxwrich

(5) US Navy Hydrographic Office. (1917). *British Islands Pilot Vol. II, The West Coast of England and Wales.* Washington, DC: Government Printing Office. Downloaded from http://books.google.com/books?id=iKouAAAAYAAJ&pg=PA373&dq=depth+of+river+clwyd